

1 Simulating the global distribution of nitrogen isotopes in the ocean

2 Christopher J. Somes,¹ Andreas Schmittner,¹ Eric D. Galbraith,² Moritz F. Lehmann,³
 3 Mark A. Altabet,⁴ Joseph P. Montoya,⁵ Ricardo M. Letelier,¹ Alan C. Mix,¹
 4 Annie Bourbonnais,⁶ and Michael Eby⁶

5 Received 13 January 2010; revised 21 June 2010; accepted 21 July 2010; published XX Month 2010.

6 [1] We present a new nitrogen isotope model incorporated into the three-dimensional
 7 ocean component of a global Earth system climate model designed for millennial
 8 timescale simulations. The model includes prognostic tracers for the two stable nitrogen
 9 isotopes, ¹⁴N and ¹⁵N, in the nitrate (NO₃⁻), phytoplankton, zooplankton, and detritus
 10 variables of the marine ecosystem model. The isotope effects of algal NO₃⁻ uptake,
 11 nitrogen fixation, water column denitrification, and zooplankton excretion are considered
 12 as well as the removal of NO₃⁻ by sedimentary denitrification. A global database of
 13 δ¹⁵NO₃⁻ observations is compiled from previous studies and compared to the model
 14 results on a regional basis where sufficient observations exist. The model is able to
 15 qualitatively and quantitatively reproduce many of the observed patterns such as high
 16 subsurface values in water column denitrification zones and the meridional and vertical
 17 gradients in the Southern Ocean. The observed pronounced subsurface minimum in the
 18 Atlantic is underestimated by the model presumably owing to too little simulated
 19 nitrogen fixation there. Sensitivity experiments reveal that algal NO₃⁻ uptake, nitrogen
 20 fixation, and water column denitrification have the strongest effects on the simulated
 21 distribution of nitrogen isotopes, whereas the effect from zooplankton excretion is
 22 weaker. Both water column and sedimentary denitrification also have important indirect
 23 effects on the nitrogen isotope distribution by reducing the fixed nitrogen inventory,
 24 which creates an ecological niche for nitrogen fixers and, thus, stimulates additional N₂
 25 fixation in the model. Important model deficiencies are identified, and strategies for
 26 future improvement and possibilities for model application are outlined.

27 **Citation:** Somes, C. J., A. Schmittner, E. D. Galbraith, M. F. Lehmann, M. A. Altabet, J. P. Montoya, R. M. Letelier, A. C. Mix,
 28 A. Bourbonnais, and M. Eby (2010), Simulating the global distribution of nitrogen isotopes in the ocean, *Global Biogeochem.*
 29 *Cycles*, 24, XXXXXX, doi:10.1029/2009GB003767.

30 1. Introduction

31 [2] Bioavailable nitrogen (fixed N) is one of the major
 32 limiting nutrients for algal photosynthesis, which drives the
 33 sequestration of CO₂ from the surface ocean and atmosphere
 34 into the deep ocean via the sinking of organic matter. Changes
 35 in this so-called “biological pump” have been hypothesized
 36 to account for a significant amount of the glacial-interglacial

fluctuations in atmospheric CO₂ [McElroy, 1983; Falkowski, 37
 1997]. However, the relative contributions of the biological 38
 and physical carbon pumps to CO₂ variations remain con- 39
 troversial. The size of the oceanic fixed N inventory, which 40
 regulates the strength of the biological pump, is controlled by 41
 different biogeochemical processes that are difficult to con- 42
 strain quantitatively in a global budget [Codispoti, 2007]. 43
 Nitrogen isotopes (both in dissolved and organic N species) in 44
 the water column and seafloor sediments are sensitive in- 45
 dicators of those processes [Brandes and Devol, 2002; 46
 Deutsch et al., 2004; Altabet, 2007]. 47

[3] Many N transformational processes alter the ratio of 48
 the two stable forms of the nitrogen isotopes, ¹⁴N and ¹⁵N, 49
 differently, a process referred to as fractionation. Resulting 50
 variations in N isotopic composition can be described as 51
 deviations in ¹⁵N/¹⁴N ratio from an accepted standard 52

$$\delta^{15}\text{N} = \left[\left(\frac{{}^{15}\text{N}}{{}^{14}\text{N}} \right) / R_{\text{std}} - 1 \right] \times 1000, \quad (1)$$

where R_{std} is the ¹⁵N/¹⁴N ratio of atmospheric N₂ gas. Iso- 53
 tope fractionation can occur due to kinetic processes (i.e., 54

¹College of Oceanic and Atmospheric Sciences, Oregon State University, Corvallis, Oregon, USA.

²Department of Earth and Planetary Science, McGill University, Montreal, Quebec, Canada.

³Institute for Environmental Geoscience, University of Basel, Basel, Switzerland.

⁴School for Marine Science and Technology, University of Massachusetts Dartmouth, North Dartmouth, Massachusetts, USA.

⁵School of Biology, Georgia Institute of Technology, Atlanta, Georgia, USA.

⁶School of Earth and Ocean Sciences, University of Victoria, Victoria, British Columbia, Canada.

55 different reaction rates for isotopes in a reactant product
56 stream). It generally results in the enrichment of the heavier
57 ^{15}N isotope in the reaction substrate, and its depletion in the
58 product. For example, preferential discrimination against
59 ^{15}N relative to ^{14}N during algal NO_3^- assimilation results in
60 net enrichment of ^{15}N in the residual NO_3^- and net depletion
61 of ^{15}N in organic matter (OM). The degree of isotopic dis-
62 crimination, or fractionation, for each process can be
63 quantified with an enrichment factor, $\varepsilon = (k^{15}/k^{14} - 1) \times$
64 1000, where k is the specific reaction rate for each isotope
65 [Mariotti et al., 1981].

66 [4] The predominant source and sink terms of the oceanic
67 fixed N inventory, N_2 fixation and denitrification, respec-
68 tively, have their own distinct effects on the signature of the
69 N isotopes in the ocean. N_2 fixing prokaryotes (diazotrophs)
70 introduce bioavailable N into the ocean close to that of
71 atmospheric N_2 ($\delta^{15}\text{N} \approx -2-0\text{‰}$) [Delwiche and Steyn,
72 1970; Minagawa and Wada, 1986; Macko et al., 1987;
73 Carpenter et al., 1997]. *Trichodesmium*, one of the most
74 important and best studied diazotrophs, bloom more fre-
75 quently and extensively in warm ($>25^\circ\text{C}$) surface water
76 where rates of aeolian Fe deposition are high such as the
77 North Atlantic, Indian, and North Pacific compared to areas
78 of low Fe deposition such as the South Pacific where the
79 abundance of *Trichodesmium* appears to be much lower
80 [Karl et al., 2002; Carpenter and Capone, 2008]. However,
81 other unicellular diazotrophs have been observed to grow in
82 cooler water near 20°C [Needoba et al., 2007], and it has
83 been suggested that they also may significantly contribute to
84 the global N_2 fixation rate [Zehr et al., 2001; Montoya et al.,
85 2004].

86 [5] Denitrification occurs under suboxic conditions ($\text{O}_2 <$
87 $5 \mu\text{mol/kg}$) in the water column and in the seafloor sedi-
88 ments. Here, microbes use NO_3^- instead of O_2 as the electron
89 acceptor during respiration and convert it to gaseous forms of
90 N (N_2O and N_2), which can then escape to the atmosphere
91 [Codispoti and Richards, 1976]. The volume and distribution
92 of suboxic water is affected by the temperature-dependent
93 solubility of O_2 at the surface and the rate of subduction of
94 oxygen-saturated water masses to greater depths, as well as
95 the amount of organic matter that remineralizes in the ocean
96 interior, both of which are sensitive to changes in climate.
97 Anammox is another important process that occurs in
98 anaerobic conditions and eliminates forms of fixed N (NO_2^- ,
99 NH_4^+) in the water column by converting them into N_2 gas
100 [Mulder et al., 1995; Thamdrup and Dalsgaard, 2002;
101 Kuypers et al., 2003]. It has been suggested that anammox
102 may even eliminate more fixed N than water column deni-
103 trification in some oxygen minimum zones [Kuypers et al.,
104 2005; Lam et al., 2009], but just how important of a role
105 anammox plays in the global fixed N inventory has yet to be
106 determined.

107 [6] Denitrifiers preferentially consume $^{14}\text{NO}_3^-$ leaving the
108 residual oceanic NO_3^- pool strongly enriched in the heavier
109 ^{15}N , with N isotope enrichment factors between 20–30‰
110 [Cline and Kaplan, 1975; Liu and Kaplan, 1989; Brandes
111 et al., 1998; Altabet et al., 1999b; Voss et al., 2001].
112 Sedimentary denitrification is generally limited by the
113 amount of NO_3^- that diffuses into the reactive zones within
114 the sediments. Therefore, it consumes nearly all of the

115 NO_3^- available, leaving nearly unaltered $\delta^{15}\text{N}$ 115
116 values in the overlying waters [Brandes and Devol, 1997, 116
2002; Sigman et al., 2003; Lehmann et al., 2004, 2007]. 117
118 The average oceanic $\delta^{15}\text{NO}_3^-$ value near 5‰ [Sigman et al.,
1997, 1999] can be interpreted as the balance between 119
120 the isotope effects of water column denitrification, sedi-
121 mentary denitrification, and N_2 fixation [Brandes and
122 Devol, 2002; Deutsch et al., 2004; Galbraith et al.,
2004; Altabet, 2007]. 123

124 [7] The $\delta^{15}\text{N}$ signal in the water column and seafloor 124
125 sediments is also affected by fractionation processes within
126 the food chain. Marine algae preferentially assimilate the
127 lighter ^{14}N into their biomass with a range of enrichment
128 factors estimated in the field between 4–15‰ [Wada, 1980;
129 Altabet et al., 1991, 1999b; Sigman et al., 1999; Altabet and
130 Francois, 2001; Karsh et al., 2003; DiFiore et al., 2006].
131 Nitrogen is not lost or gained from the ocean during algal
132 NO_3^- assimilation, but the spatial separation between net
133 assimilation and remineralization can cause a trend of
134 decreasing $\delta^{15}\text{NO}_3^-$ with depth. Distinguishing between the
135 different isotope effects remains a challenge, especially in
136 regions where multiple N transformational processes are
137 occurring within close proximity.

138 [8] This study, for the first time to our knowledge, includes 138
139 a dynamic nitrogen isotope module embedded within an
140 existing global ocean-atmosphere-sea ice-biogeochemical
141 model. This allows a direct comparison with nitrogen isotope
142 observations, whereas previous box model studies could
143 only be used more qualitatively [Giraud et al., 2000;
144 Deutsch et al., 2004]. We provide a detailed description
145 of the nitrogen isotope model and an assessment of its
146 skill in reproducing present-day $\delta^{15}\text{NO}_3^-$ observations.
147 Comparison of model results with $\delta^{15}\text{N}$ observations will
148 also be used to help to quantify processes that affect the
149 global oceanic distribution of $\delta^{15}\text{N}$. Sensitivity experi-
150 ments illustrate the individual isotope effects of different
151 processes on the spatial distribution of the N isotopes. In
152 combination with measurements in ocean sediments and
153 in the water column, the model can be a tool to better
154 understand variations of $\delta^{15}\text{N}$ and the nitrogen cycle in
155 the past and present.

2. Model Description 156

2.1. Physical Model 157

158 [9] The physical model is based on the University of 158
159 Victoria Earth system climate model [Weaver et al., 2001],
160 version 2.8. It includes a global, three-dimensional general
161 circulation model of the ocean (Modular Ocean Model 2)
162 with physical parameterizations such as diffusive mixing
163 along and across isopycnals, eddy induced tracer advection
164 [Gent and McWilliams, 1990] and a scheme for the compu-
165 tation of tidally induced diapycnal mixing over rough
166 topography [Simmons et al., 2004]. Nineteen vertical levels
167 are used with a horizontal resolution of $1.8^\circ \times 3.6^\circ$. To
168 improve the simulation of equatorial currents, we have
169 increased the meridional resolution in the tropics to 0.9°
170 (between 10°S and 10°N and smoothly transitioning to 1.8°
171 at 20°N/S) and added an anisotropic viscosity scheme
172 [Large et al., 2001]. A more detailed description of this

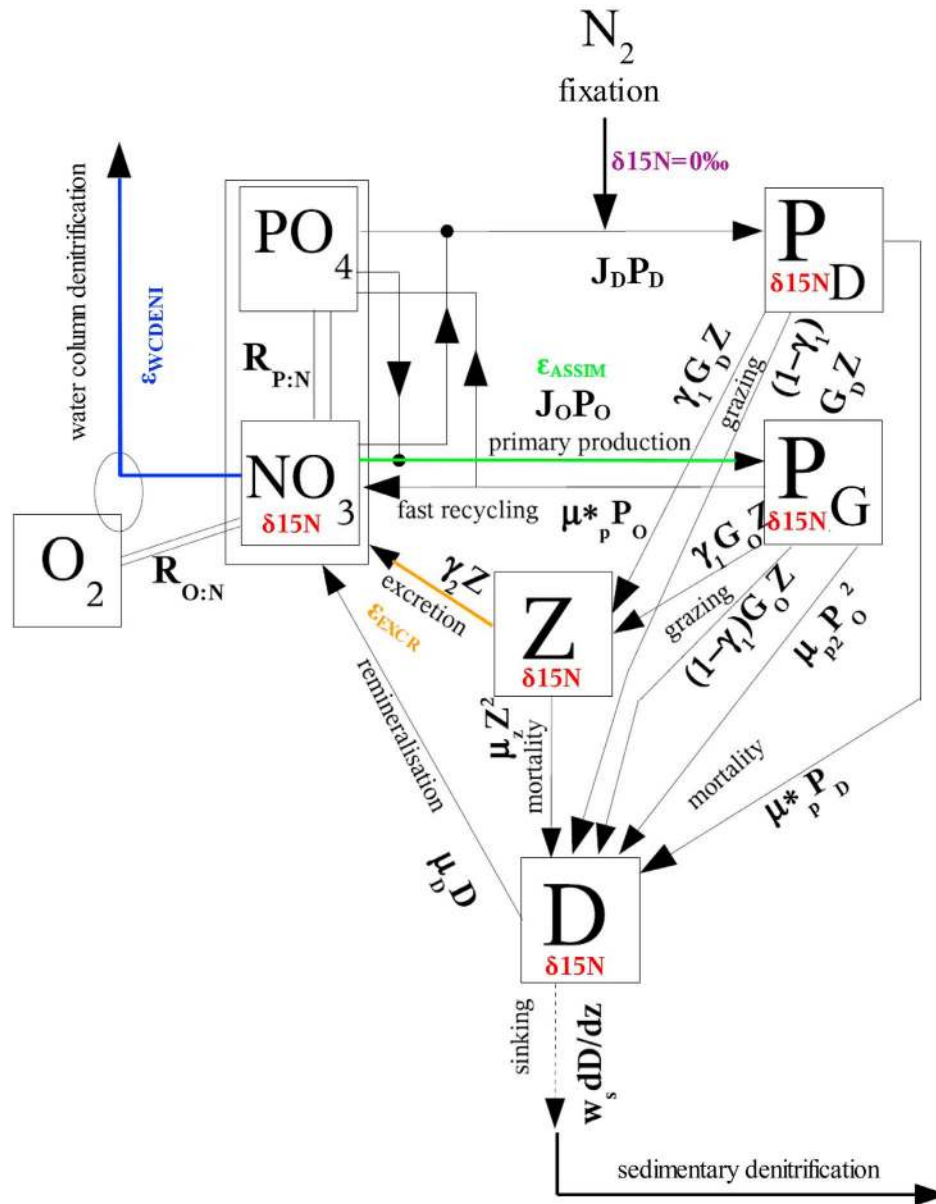


Figure 1. Schematic of the marine ecosystem model with the nitrogen isotope model parameters in color.

173 parameterization and its effect on the equatorial circulation
 174 is provided in Text S1 of the auxiliary material.¹ To account
 175 for the overestimated ventilation in the North Pacific, an
 176 artificial stratifying force equal to 0.04 Sv of freshwater is
 177 applied over the surface north of 55° in the Pacific and
 178 compensated elsewhere. A two dimensional, single level
 179 energy-moisture balance model of the atmosphere and a
 180 state-of-the-art dynamic-thermodynamic sea ice model are
 181 used, forced with prescribed NCEP/NCAR monthly clima-
 182 tological winds.

¹Auxiliary materials are available in the HTML. doi:10.1029/2009GB003767.

2.2. Marine Ecosystem Model

183

[10] The marine ecosystem model is an improved version
 184 of the NPZD (Nutrient, Phytoplankton, Zooplankton,
 185 Detritus) ecosystem model of [Schmittner *et al.*, 2008]
 186 (Figure 1). The organic variables include two classes of
 187 phytoplankton, N_2 fixing diazotrophs (P_D) and a “general”
 188 NO_3^- assimilating phytoplankton class (P_G), as well as
 189 zooplankton (Z) and organic detritus (D). The inorganic
 190 variables include dissolved oxygen (O_2) and two nutrients,
 191 nitrate (NO_3^-) and phosphate (PO_4^{3-}), both of which are
 192 consumed by phytoplankton and remineralized in fixed
 193 elemental ratios ($R_{N:P} = 16$, $R_{O:P} = 170$). We note, though,
 194

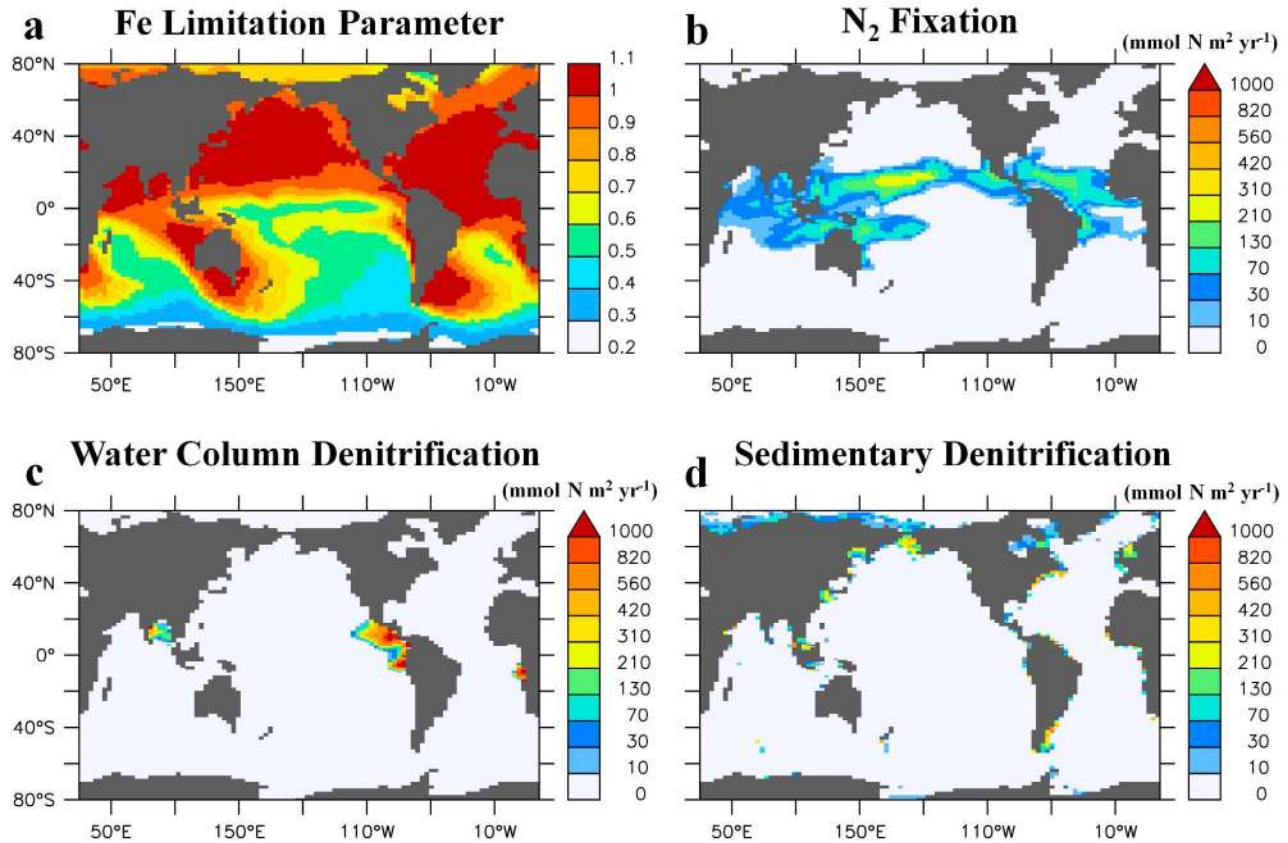


Figure 2. (a) Fe limitation parameter based on an estimate of aeolian dust deposition [Mahowald *et al.*, 2005] which is multiplied to the maximum growth rate of diazotrophs (see text). Annual vertically integrated rates of (b) N₂ fixation, (c) water column denitrification, and (d) sedimentary denitrification.

195 that most diazotrophs have been found to have a $R_{N:P}$ of
 196 50:1 and sometimes higher [e.g., *Letelier and Karl*, 1996,
 197 1998]. This simplification is one of the reasons why the
 198 nitrogen surplus $N' = NO_3^- - 16PO_4^{3-}$ is generally under-
 199 estimated in surface waters in the model (Figure S3). In
 200 addition to water column denitrification and N₂ fixation, we
 201 now include a parameterization for sedimentary denitrifi-
 202 cation (see auxiliary material equation (S11) and Figure 2),
 203 based on the flux of organic carbon into the seafloor sedi-
 204 ments [Middelburg *et al.*, 1996]. Since the model under-
 205 estimates coastal upwelling, which drives large fluxes of
 206 organic carbon to the seafloor sediments, this parameteri-
 207 zation is tuned to fit the global mean $\delta^{15}NO_3^-$ of 5‰ by
 208 multiplying the sedimentary denitrification equation by a
 209 constant factor ($\alpha_{SD} = 6.5$). Global rates of model N₂ fix-
 210 ation, water column denitrification, and sedimentary deni-
 211 trification are 102, 78.0, and 25.4 Tg N yr⁻¹, respectively.
 212 The relatively low model sedimentary to water column
 213 denitrification ratio of ~1:3 compared to other estimates
 214 from one-box models ranging from ~1:1 [Altabet, 2007] to
 215 ~4:1 [Brandes and Devol, 2002] is mostly due to the
 216 “dilution effect” [Deutsch *et al.*, 2004], which reduces the
 217 “effective” fractionation effect of water column denitrifica-
 218 tion as NO₃⁻ is locally consumed, an effect not incorporated
 219 in one-box models. This results in a lower sedimentary to

water column denitrification ratio needed to set the global
 mean $\delta^{15}NO_3^-$ to 5‰ (see section 4.2 for further discus-
 sion). The complete marine ecosystem model description is
 provided in Text S2 of the auxiliary material. A compar-
 ison of the global distribution of NO₃⁻, O₂, and N' with
 World Ocean Atlas 2005 (WOA05) observations is shown
 in Figure S3.

[11] Suboxic water, where water column denitrification
 occurs, is present in three main locations of the present-day
 oceans: the Eastern Tropical North Pacific (ETNP), the
 Eastern Tropical South Pacific (ETSP) and the Arabian Sea
 (Figure S3). Deficiencies in the physical circulation model
 simulate suboxic water in only one of these locations, the
 ETNP. The physical circulation model integrates coastal
 upwelling over a horizontal extent that is too large (due to its
 coarse resolution), which results in the underestimation of
 upwelling, export production, and the remineralization of
 organic matter at depth. This bias leads to too high O₂
 concentrations, larger than required for water column deni-
 trification, in the ETSP and the Arabian Sea. Suboxia in the
 so-called “shadow zone” of the ETNP is simulated better
 and investigated more in section 4.2. In the model, some
 water column denitrification also occurs in the Bay of
 Bengal and off SW Africa (Figure 2c), which has not been
 observed in the real ocean. However, the anammox reaction,

t1.1 **Table 1.** Nitrogen Isotope Model Enrichment Factors

t1.2	Process	Symbol	Model Enrichment Factor (‰)	Field Estimates ^a (‰)
t1.3	Algal NO ₃ assimilation	ϵ_{ASSIM}	5	4–15
t1.4	N ₂ fixation	ϵ_{NFIX}	1.5	0–2
t1.5	Excretion	ϵ_{EXCR}	6	3–6
t1.6	Water column denitrification	ϵ_{WCD}	25	22–30
t1.7	Sedimentary denitrification	ϵ_{SD}	0	0–4

t1.8 ^aSee Appendix A for references.

245 which also eliminates fixed N in the water column, has
 246 been found to occur off SW Africa [Kuypers *et al.*, 2005].
 247 Naqvi [2008] measured low decomposition rates in the Bay
 248 of Bengal. Effective ballasting and scavenging of organic
 249 matter by the massive riverine input of terrestrial matter, an
 250 effect not included in the model, may prevent water col-
 251 umn denitrification in the Bay of Bengal, which is close to
 252 suboxic.

253 [12] Diazotrophs grow according to the same principles as
 254 algal phytoplankton in the model (see Text S2), but we also
 255 account for some of their different characteristics. N₂ fixa-
 256 tion breaks down of the triple N bond of N₂, which is
 257 energetically more costly than assimilating fixed N [Holl
 258 and Montoya, 2005]. Therefore, in the model, the growth
 259 rate of diazotrophs is lower than that of general phyto-
 260 plankton. It is zero in waters cooler than 15°C and increases
 261 50% slower with temperature than the growth rate of general
 262 phytoplankton. Diazotrophs are not limited by NO₃⁻ and will
 263 thrive in waters that are N deficient (i.e., low N' as a result of
 264 denitrification) in which sufficient P and Fe are available.
 265 Denitrification and the propagation of N-deficient waters
 266 into the shallow thermocline by physical transport processes
 267 create an ecological niche for diazotrophs in the model,
 268 which stimulates N₂ fixation [Tyrrell, 1999].

269 [13] One of the most important and best studied diazo-
 270 trophs, *Trichodesmium*, also has large iron (Fe) require-
 271 ments for growth [Sañudo-Wilhelmy *et al.*, 2001].
 272 Diazotrophs may depend on aeolian Fe in oligotrophic
 273 waters because deep pycnocline inhibits upward mixing of
 274 subsurface Fe-replete waters into the euphotic zone
 275 [Falkowski, 1997; Karl *et al.*, 2002]. Therefore, their growth
 276 rate is further reduced according to the *Fe Limitation*
 277 parameter (Figure 2a), where an estimate of aeolian dust
 278 deposition [Mahowald *et al.*, 2005] is scaled between 0–1
 279 by multiplying it by a constant factor and setting the max-
 280 imum value to 1. This is a simple parameterization of Fe
 281 limitation of diazotrophy and its full effects are described
 282 elsewhere [Somes, 2010]. The majority of N₂ fixation in the
 283 model occurs in oligotrophic waters “downstream” of
 284 denitrification zones where sufficient Fe exists (i.e., via
 285 aeolian Fe deposition) (Figure 2b). The pattern of N₂ fixa-
 286 tion (such as high values in the tropical/subtropical North
 287 Pacific, the western tropical/subtropical South Pacific, the
 288 western tropical/subtropical South Atlantic, the tropical/
 289 subtropical North Atlantic and the Indian Ocean) is mostly
 290 consistent with direct observations [e.g., Karl *et al.*, 2002;
 291 Carpenter and Capone, 2008], with estimates based on the
 292 observed NO₃⁻ deficit and simulated circulation [Deutsch

et al., 2007], as well as with results from a more com- 293
 294 plex ecosystem model [Moore and Doney, 2007]. How-
 295 ever, N₂ fixation in our model does not extend northward
 296 of 25–30°N in the North Pacific and North Atlantic,
 297 whereas some observations show N₂ fixation as far north
 298 as 35–40°N [Church *et al.*, 2008; Kitajima *et al.*, 2009].

2.3. Nitrogen Isotope Model 299

[14] The nitrogen isotope model simulates the distribution 300
 301 of the two stable nitrogen isotopes, ¹⁴N and ¹⁵N, in all N
 302 species throughout the global ocean that are included in the
 303 marine ecosystem model. Five prognostic variables of $\delta^{15}\text{N}$
 304 are embedded within the marine ecosystem model for all
 305 species containing nitrogen: NO₃⁻, diazotrophs, algal phy-
 306 toplankton, zooplankton and organic detritus (Figure 1). The
 307 ‘isotope effect’ is referred to in the following as the effect
 308 that each process has on the respective oceanic isotopic N
 309 pool, which depends on the $\delta^{15}\text{N}$ value of the substrate, the
 310 process-specific enrichment factor (ϵ), and the degree of
 311 utilization ($u_{\text{substrate}}$) of the substrate during the reaction:

$$\delta^{15}\text{N}_{\text{product}} = \delta^{15}\text{N}_{\text{substrate}} - \epsilon(1 - u_{\text{substrate}}), \quad (2)$$

where $u_{\text{substrate}}$ is the fraction of the initial substrate used in 312
 313 the reaction. For example, if all of the available substrate is
 314 consumed in the reaction (i.e., $u_{\text{substrate}} = 1$), the product will
 315 incorporate the $\delta^{15}\text{N}$ value of the substrate, nullifying any
 316 potential fractionation. However, if the rate of utilization is
 317 low (i.e., $u_{\text{substrate}} \sim 0$), the product will incorporate a rela-
 318 tively light $\delta^{15}\text{N}$ value compared to the substrate by the
 319 designated enrichment factor (Table 1).

[15] The processes in the model that fractionate nitrogen 320
 321 isotopes are algal NO₃⁻ assimilation ($\epsilon_{\text{ASSIM}} = 5\text{‰}$), zoo-
 322 plankton excretion ($\epsilon_{\text{EXCR}} = 6\text{‰}$), and water column deni-
 323 trification ($\epsilon_{\text{WCD}} = 25\text{‰}$) (Table 1). Fractionation results in
 324 the isotopic enrichment of the more reactive, thermody-
 325 namically preferred, light ¹⁴N into the product of each
 326 reaction by a process-specific fractionation factor. For a
 327 detailed discussion of nitrogen isotope fractionation
 328 dynamics see [Mariotti *et al.*, 1981]. Although little frac-
 329 tionation occurs during N₂ fixation in the model, it has an
 330 important effect on $\delta^{15}\text{N}$ by introducing relatively light
 331 atmospheric N₂ ($\delta^{15}\text{N} = 0\text{‰}$) into the oceanic fixed N
 332 inventory. Sedimentary denitrification also has been
 333 observed to have little effect on the oceanic isotopic N pool
 334 because denitrifiers consume nearly all NO₃⁻ diffusing into
 335 the sediments [Brandes and Devol, 1997, 2002; Lehmann
 336 *et al.*, 2004, 2007]. In the model, there is no fractionation
 337 during sedimentary denitrification ($\epsilon_{\text{SD}} = 0\text{‰}$), although this
 338 is a simplification of observations [Lehmann *et al.*, 2007].
 339 Fractionation during the remineralization of organic matter is
 340 not included in the model. The complete nitrogen isotope
 341 model description is provided in Appendix A.

3. Nitrogen Isotope Model Results 342

[16] The model simulates complex spatial patterns of 343
 344 $\delta^{15}\text{NO}_3^-$ and $\delta^{15}\text{N}$ organic matter (OM) throughout the
 345 global ocean (top panels of Figure 3). Patterns of surface
 346 $\delta^{15}\text{NO}_3^-$ and subsurface $\delta^{15}\text{N}$ OM are very similar but values

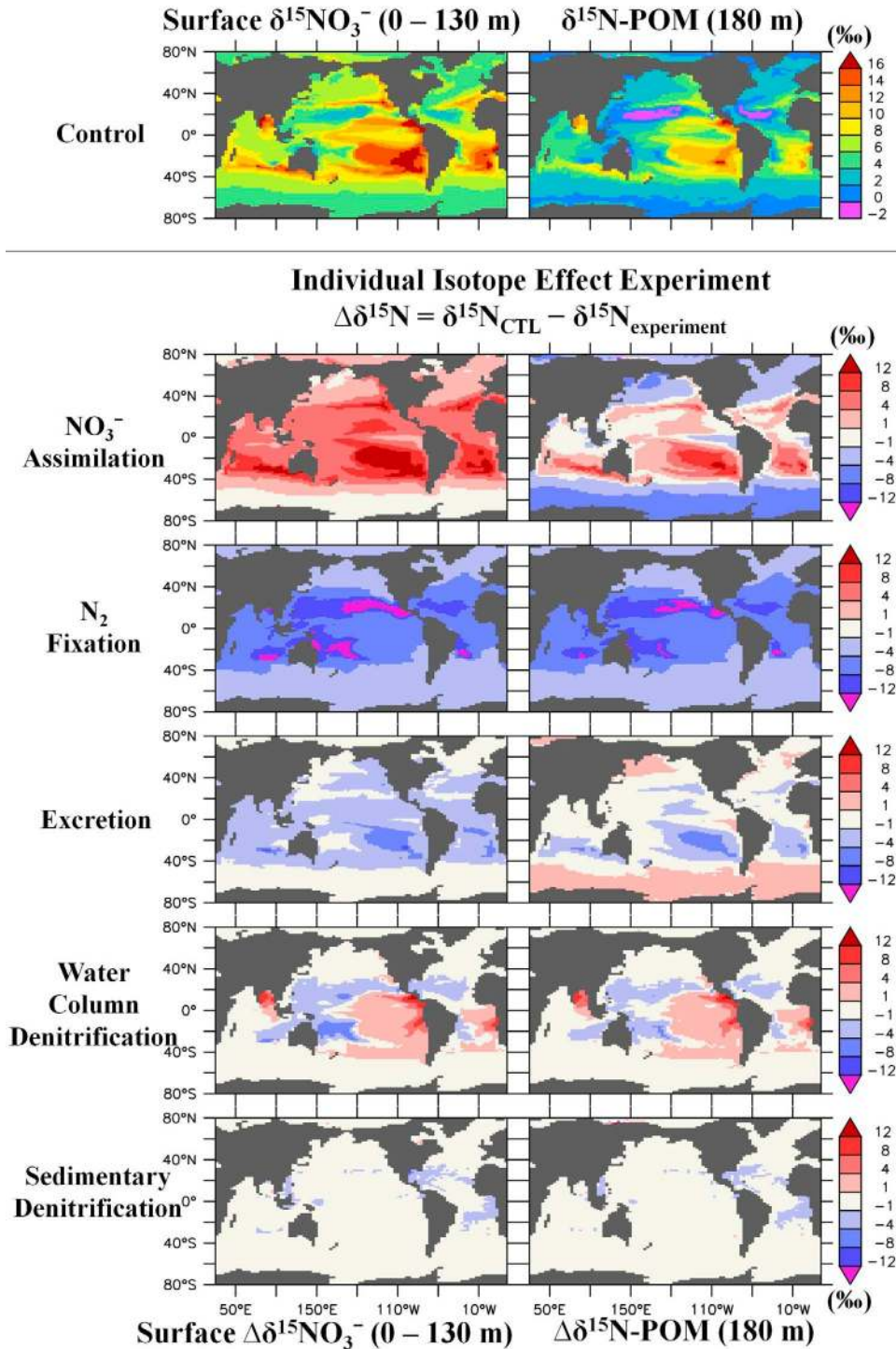


Figure 3. (top) Surface $\delta^{15}\text{NO}_3^-$ and $\delta^{15}\text{N}$ of sinking detritus in the model. (bottom) Isotope effect sensitivity experiments where one isotope effect is neglected per simulation and its difference with CTL is shown to illustrate its individual effect on the CTL simulation.

347 are offset by two processes. First, as much as 5‰ offset due
 348 to fractionation during NO_3^- uptake by phytoplankton and
 349 second, by fractionation during zooplankton excretion,
 350 which increases the $\delta^{15}\text{N}$ OM through zooplankton mor-

351 tality (Figure 1). High $\delta^{15}\text{NO}_3^-$ values ($>15\text{‰}$) are simulated
 352 in the eastern subtropical gyres, where surface NO_3^- is
 353 depleted, and in regions in close proximity to simulated
 354 suboxic zones in the Eastern Pacific, Bay of Bengal, and

355 Eastern Atlantic (again, note that water column denitrifi-
 356 cation has not been actually observed in the Bay of Bengal
 357 and Eastern Atlantic). A clear interhemispheric asymmetry
 358 appears between the subtropical gyres of the Pacific and
 359 Atlantic with higher values of 14–20‰ simulated in the
 360 southern hemisphere and smaller values of 10–14‰ in the
 361 northern hemisphere. More intermediate $\delta^{15}\text{N}$ values of
 362 4–8‰ are found at high latitudes and near the equator
 363 where nutrient utilization is incomplete. $\delta^{15}\text{N}$ minima
 364 (<4‰) are located in the western tropical/subtropical ocean
 365 basins, where N_2 fixation occurs in the model (Figure 2b).
 366 The remainder of this section presents a more quantitative
 367 description of the contributions of individual processes to
 368 these relatively complex spatial patterns of $\delta^{15}\text{NO}_3^-$ and
 369 $\delta^{15}\text{N}$ OM.

370 [17] Figure 3 illustrates results from the full model (CTL)
 371 that includes all isotope effects (top panels) together with
 372 results from sensitivity experiments designed to isolate the
 373 effects of individual processes (bottom panels) on the global
 374 $\delta^{15}\text{N}$ distribution. This is accomplished by removing the
 375 isotope effect of one process per experiment and then
 376 calculating the difference ($\Delta\delta^{15}\text{N}$) with CTL. In the “ NO_3^-
 377 Assimilation” and “Excretion” experiments, the enrichment
 378 factors $\varepsilon_{\text{ASSIM}}$ and $\varepsilon_{\text{EXCR}}$, respectively, are set to zero. In
 379 the “ N_2 fixation” experiment the diazotroph’s N isotope
 380 ratio is set equal to that of other phytoplankton at each
 381 location. In the “Water Column Denitrification” and
 382 “Sedimentary Denitrification” experiments, the entire pro-
 383 cess is switched off (thereby changing the global N
 384 inventory). These latter experiments also show the indirect
 385 effect that both denitrification processes have on $\delta^{15}\text{N}$
 386 through the stimulation of N_2 fixation. In all other isotope
 387 effect experiments, the total N inventory does not change.

388 3.1. Algal NO_3^- Assimilation

389 [18] As phytoplankton preferentially assimilate $^{14}\text{NO}_3^-$
 390 into organic matter, they leave the residual inorganic N pool
 391 enriched in $^{15}\text{NO}_3^-$. This creates an offset between surface
 392 $\delta^{15}\text{NO}_3^-$ and $\delta^{15}\text{N}$ OM that sinks toward the seafloor, which is
 393 set by the enrichment factor for NO_3^- assimilation ($\varepsilon_{\text{ASSIM}} =$
 394 5‰) (“ NO_3^- Assimilation” experiment, Figure 3). The
 395 surface NO_3^- utilization effect is also affected by the
 396 extent to which NO_3^- is depleted. When NO_3^- utilization is
 397 low (i.e., NO_3^- -replete water exists), which occurs in High
 398 Nitrate Low Chlorophyll (HNLC) regions such as the
 399 Southern Ocean, the subarctic North Pacific, and the eastern
 400 equatorial Pacific, surface $\delta^{15}\text{NO}_3^-$ is determined by the
 401 source of $\delta^{15}\text{NO}_3^-$ being supplied to the surface. Algae will
 402 fractionate this NO_3^- during assimilation near the full extent
 403 set by the designated enrichment factor because of the
 404 abundance of available NO_3^- . In this oceanographic setting,
 405 the expected 5‰ difference between $\delta^{15}\text{NO}_3^-$ and $\delta^{15}\text{N}$ OM
 406 is almost fully expressed (i.e., $\delta^{15}P_G = \delta^{15}\text{NO}_3^- - \varepsilon_{\text{ASSIM}}$ with
 407 $u_{\text{ASSIM}} \approx 0$ in equation (2)). Thus, surface NO_3^- utilization in
 408 HNLC regions has a small influence on the surface $\delta^{15}\text{NO}_3^-$
 409 signature, but play an important role for $\delta^{15}\text{N}$ OM that sinks
 410 out of the euphotic zone. This is perhaps most obvious in the
 411 Southern Ocean and in the subarctic North Pacific where
 412 $\Delta\delta^{15}\text{NO}_3^-$ is small, whereas $\Delta\delta^{15}\text{N}$ OM is strongly negative
 413 (“ NO_3^- Assimilation” experiment, Figure 3).

[19] A different response is observed in oligotrophic re- 414
 gions where surface NO_3^- is depleted. Once the algae con- 415
 sume nearly all available NO_3^- (which itself becomes 416
 enriched in ^{15}N), they acquire the same N isotope signature 417
 from the source NO_3^- (i.e., $\delta^{15}P_G = \delta^{15}\text{NO}_3^-$ with u_{ASSIM} 418
 approaching 1). This drives the high $\delta^{15}\text{N}$ values in both 419
 NO_3^- and OM in the subtropics with maxima in the eastern 420
 poleward edges of the gyres (Figure 3). Although $\delta^{15}\text{NO}_3^-$ 421
 values are very high there, they have a small effect on $\delta^{15}\text{N}$ 422
 elsewhere because NO_3^- concentrations are very low. For 423
 instance, when low NO_3^- water mixes with nearby water 424
 with significantly higher NO_3^- , the resulting $\delta^{15}\text{NO}_3^-$ value 425
 will be weighted toward the water parcel containing more 426
 NO_3^- [see also *Deutsch et al.*, 2004]. This ‘dilution effect’ 427
 prevents high $\delta^{15}\text{NO}_3^-$ values in regions with high surface 428
 NO_3^- utilization from having a large impact on the $\delta^{15}\text{NO}_3^-$ 429
 signature across the nitracline. 430

3.2. Denitrification 431

[20] Denitrification only occurs at depth but its isotope 432
 effect can reach the surface due to upwelling and vertical 433
 mixing. Water column denitrification has a large enrich- 434
 ment factor and displays a very strong N isotope effect in 435
 close proximity to the simulated suboxic zones in the 436
 Eastern Pacific, Bay of Bengal, and Eastern Atlantic 437
 (“Water Column Denitrification” experiment in Figure 3). 438
 The unresolved poleward undercurrents along the western 439
 continental margin of the Americas (which could, in the 440
 real world, propagate high $\delta^{15}\text{NO}_3^-$ away from the sub- 441
 surface suboxic zones [*Kienast et al.*, 2002]) may restrict 442
 the simulated water column denitrification isotope effect 443
 too much to regions proximal to the suboxic zones. Both 444
 water column and sedimentary denitrification also indi- 445
 rectly lead to lower $\delta^{15}\text{NO}_3^-$ values “downstream” of 446
 denitrification zones because they create N-deficient water 447
 that stimulates additional N_2 fixation, which introduces low 448
 $\delta^{15}\text{N}$ into the ocean. This negative feedback also decreases 449
 the horizontal extension of high $\delta^{15}\text{NO}_3^-$ signature origi- 450
 nating from suboxic zones, because N_2 fixation introduces 451
 much lower $\delta^{15}\text{N}$ into the ocean. 452

3.3. N_2 Fixation 453

[21] The addition of newly fixed, isotopically light 454
 atmospheric N_2 ($\delta^{15}\text{N}_2 = 0$) by diazotrophs is the reason for 455
 the low $\delta^{15}\text{N}$ values in the western tropical/subtropical 456
 ocean basins. Since denitrification is the only process in the 457
 model that creates N-deficient water, and therefore an eco- 458
 logical niche for diazotrophs, the majority of N_2 fixation in 459
 the model occurs “downstream” of denitrification zones 460
 after phytoplankton have consumed all remaining surface 461
 NO_3^- and where sufficient aeolian Fe deposition exists. This 462
 low $\delta^{15}\text{NO}_3^-$ signature is evident in the subtropical North/ 463
 South Pacific, the subtropical North/South Atlantic, and the 464
 Bay of Bengal (“ N_2 Fixation” experiment, Figure 3). 465

3.4. Excretion 466

[22] According to our model results, the N isotope effect 467
 of excretion has a smaller influence on the simulated dis- 468
 tribution of $\delta^{15}\text{N}$ in the global ocean (“Excretion” experi- 469
 ment, Figure 3) compared to the other processes discussed 470

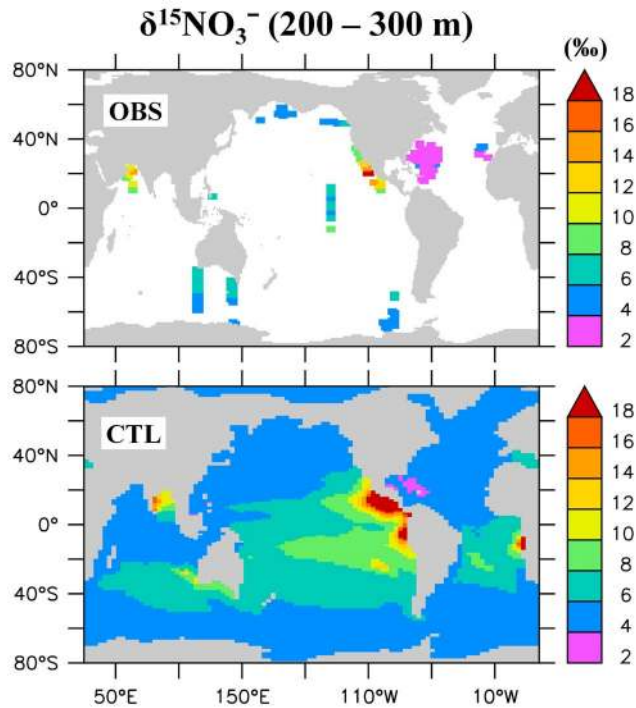


Figure 4. Comparison of annual $\delta^{15}\text{NO}_3^-$ (‰) averaged between 200 m and 300 m of available observations (OBS) and CTL. Because of the incomplete temporal coverage, seasonal biases in the annually averaged data exist depending on the region.

above. Its strongest effect is observed in the subtropical South Pacific, where NO_3^- is very low and excretion significantly contributes to the NO_3^- pool by introducing relatively low $\delta^{15}\text{NO}_3^-$. Low-latitude surface waters elsewhere are generally about 1–4‰ lighter due to fractionation during excretion, with little spatial gradients. At high latitudes the effect on $\delta^{15}\text{NO}_3^-$ is very small. We note that this N isotope effect is sensitive to the parameterization for excretion used in this marine ecosystem model version. The excretion rate was tuned so that $\delta^{15}\text{N}$ zooplankton is enriched by $\sim 3.4\%$ relative to phytoplankton [Minagawa and Wada, 1984].

4. Model Evaluation

[23] The relatively small number of $\delta^{15}\text{N}$ observations and the sparse spatial and temporal coverage make a full global model assessment difficult. However, certain regions have been sampled sufficiently to provide a meaningful comparison with the model results. All observations presented here are interpolated horizontally onto a $0.9^\circ \times 1.8^\circ$ grid using a Gaussian weighted algorithm. The 33 depth levels are consistent with WOA05 and a linear interpolation is used for depths of missing data if nearby data exist. A global database of $\delta^{15}\text{NO}_3^-$ measurements has thus been constructed and is available for download (<http://mkg.coas.oregonstate.edu/~andreas/Nitrogen/data.html>). Figure 4 shows the annually averaged global distribution of measured $\delta^{15}\text{NO}_3^-$, averaged

over 200–300 m depth to illustrate the spatial coverage. Seasonal sampling biases exist depending on the region. More details on the data sets can be found in the respective ocean region subsections that follow. Comparisons are presented for the Southern Ocean (Indian-Pacific sector), the Eastern Tropical North Pacific, the Central Equatorial Pacific and the Subtropical North Atlantic. Other regions with available $\delta^{15}\text{NO}_3^-$ observations included in the data set but not discussed in the text are the Bering Sea [Lehmann et al., 2005], the Northeast Pacific [Galbraith, 2006], the Arabian Sea [Altabet et al., 1999a] and the eastern Pacific sector of the Southern Ocean [Sigman et al., 1999].

[24] Global measures of model performance for $\delta^{15}\text{NO}_3^-$ are presented in Table 2. These measures should be interpreted taken into account the highly localized nature of some of the processes as well as the limited regions covered by the database. A displacement in the location of denitrification, for example, will lead to a large decrease in the correlation coefficient and a large increase in the RMS errors. The CTL model has a correlation coefficient of 0.68, implying that the model explains 46% of the variance in the observations. The decrease of the correlation coefficient and the increase of the RMS error due to the neglect of a particular process can be regarded as the importance that this process plays in explaining the global $\delta^{15}\text{NO}_3^-$ observations of the database. The correlation coefficient measures the pattern of variability and neglects the absolute values, whereas the RMS error considers the deviation of the model from the observations in absolute values. Neglecting water column denitrification leads to the largest decrease in the correlation coefficient to 0.29 and to the second largest increase in the RMS error after N_2 fixation. Neglecting N_2 fixation and algal NO_3^- assimilation lead to the next largest decrease in the correlation coefficient. If sedimentary denitrification or excretion is not included, then the correlation coefficients decrease similarly, with both having relatively weaker effects on the distribution of $\delta^{15}\text{NO}_3^-$. Then, according to these measures, water column denitrification is the most important process determining the global $\delta^{15}\text{NO}_3^-$ distribution of available observations in the database, followed by N_2 fixation and algal NO_3^- assimilation, respectively. Finally, sedimentary denitrification and excretion are the least important.

4.1. Southern Indian-Pacific Ocean

[25] The Southern Ocean represents a critical region of biogeochemical cycling in the ocean because it is the largest open ocean region with incomplete drawdown of the major nutrients. This results in an excess amount of CO_2 at the

Table 2. Global Measures of $\delta^{15}\text{NO}_3^-$ Model Performance^a

Model	r	P	RMS
Control	0.68	<0.0001	0.73
Algal NO_3^- assimilation	0.60	0.00046	0.85
N_2 fixation	0.52	0.0026	2.1
Excretion	0.65	0.00010	0.80
Water column denitrification	0.29	0.12	1.1
Sedimentary denitrification	0.64	0.00010	0.82

^aCorrelation coefficient (r), correlation significance (P), and root mean squared (RMS) error normalized by the standard deviation of the observations.

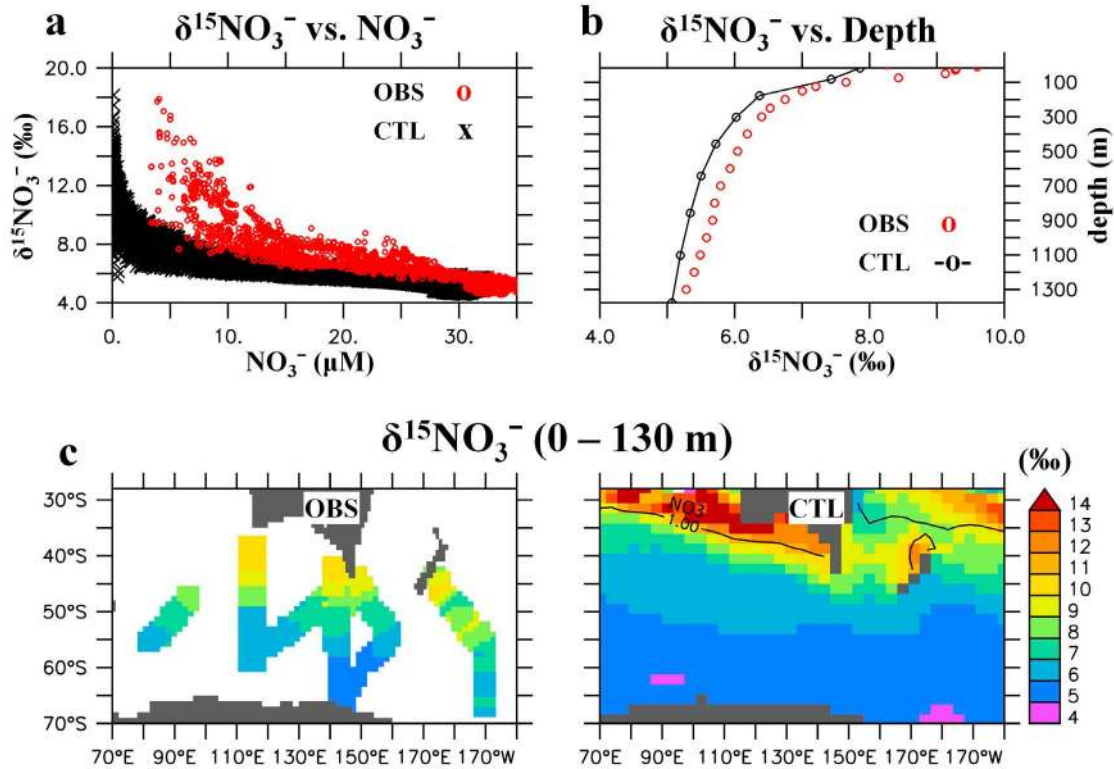


Figure 5. Comparison of the Indian-Pacific sector of the Southern Ocean with the $\delta^{15}\text{NO}_3^-$ database and CTL: (a) $\delta^{15}\text{NO}_3^-$ versus NO_3^- , (b) horizontally averaged (over available data) depth $\delta^{15}\text{NO}_3^-$ profiles, and (c) surface $\delta^{15}\text{NO}_3^-$ and with a $1\mu\text{M}$ NO_3^- contour line.

543 surface, which is released to the atmosphere (under prein-
544 dustrial conditions). The degree to which surface nutrients
545 are utilized here may have profound impacts on ocean-
546 atmosphere exchanges of CO_2 . Figure 5 shows a compari-
547 son with observations recorded in the region [Sigman *et al.*,
548 1999; Altabet and Francois, 2001; DiFiore *et al.*, 2006].
549 This data subset compiles observations from 8 cruises
550 covering various seasons. Since all cruises do not cover the
551 same location, some seasonal biases can be expected, yet,
552 we still decided to use annual averages for maximum spatial
553 coverage. The model does not simulate interannual vari-
554 ability due to the prescribed monthly climatological winds
555 and temporally constant biogeochemical parameters.

556 [26] Qualitatively, the inverse trend of increasing $\delta^{15}\text{NO}_3^-$
557 with decreasing NO_3^- (Figure 5a) is reproduced by the
558 model. However, the slope is underestimated suggesting that
559 the enrichment factor for algal NO_3^- assimilation used in the
560 model ($\epsilon_{\text{ASSIM}} = 5\text{‰}$) is too low, in agreement with
561 [DiFiore *et al.*, 2006] that suggests at least 7‰. The sim-
562 ulated vertical gradient is in good agreement with the ob-
563 servations. Deep water $\delta^{15}\text{NO}_3^-$ at 2000 m depth is around
564 5‰ and slowly increasing throughout the lower pycnocline
565 to around 6‰ at 500 m depth. The model slightly over-
566 estimates $\delta^{15}\text{NO}_3^-$ between 200 m and 400 m depth, whereas
567 near surface values are slightly underestimated.

568 [27] A large discrepancy between simulated and obser-
569 vational $\delta^{15}\text{NO}_3^-$ is apparent in surface waters north of 40°S

off the southern coast of Australia (Figure 5c). This bias is
570 due to the fact that the model overestimates the utilization of
571 surface NO_3^- relative to observations there (Figure 5c).
572 Where the simulated NO_3^- is almost completely consumed
573 (i.e., $\text{NO}_3^- < 1\mu\text{M}$) (see Figure 5c contour line), the remain-
574 ing $\delta^{15}\text{NO}_3^-$ values become as high as 18‰. Since
575 none of the existing $\delta^{15}\text{NO}_3^-$ observations was collected in
576 such low NO_3^- concentrations (Figure 5a), it is impossible, at
577 this time, to falsify this aspect of the N isotope model
578 response. We note this heavy $\delta^{15}\text{NO}_3^-$ signature in these
579 low NO_3^- waters has little effect on $\delta^{15}\text{NO}_3^-$ across the
580 nitracline in the model because the $\delta^{15}\text{N}$ signature of very
581 low NO_3^- water becomes diluted out as it mixes with much
582 higher NO_3^- water (see section 3.1).
583

4.2. Eastern Tropical North Pacific

584
585 [28] The ETNP contains the largest suboxic zone in the
586 ocean, where water column denitrification occurs. The rela-
587 tively small spatial scale of suboxic zones makes them
588 difficult for the model to simulate accurately and deficiencies
589 in the coarse resolution physical model prevent it from
590 fully resolving some important physical processes, espe-
591 cially in coastal regions. Underestimating coastal upwelling
592 (due to coarse resolution) results in corresponding under-
593 estimation of primary production, organic matter remineral-
594 ization, and O_2 consumption at depth. This is a major
595 reason for overestimated dissolved O_2 at depth in areas with

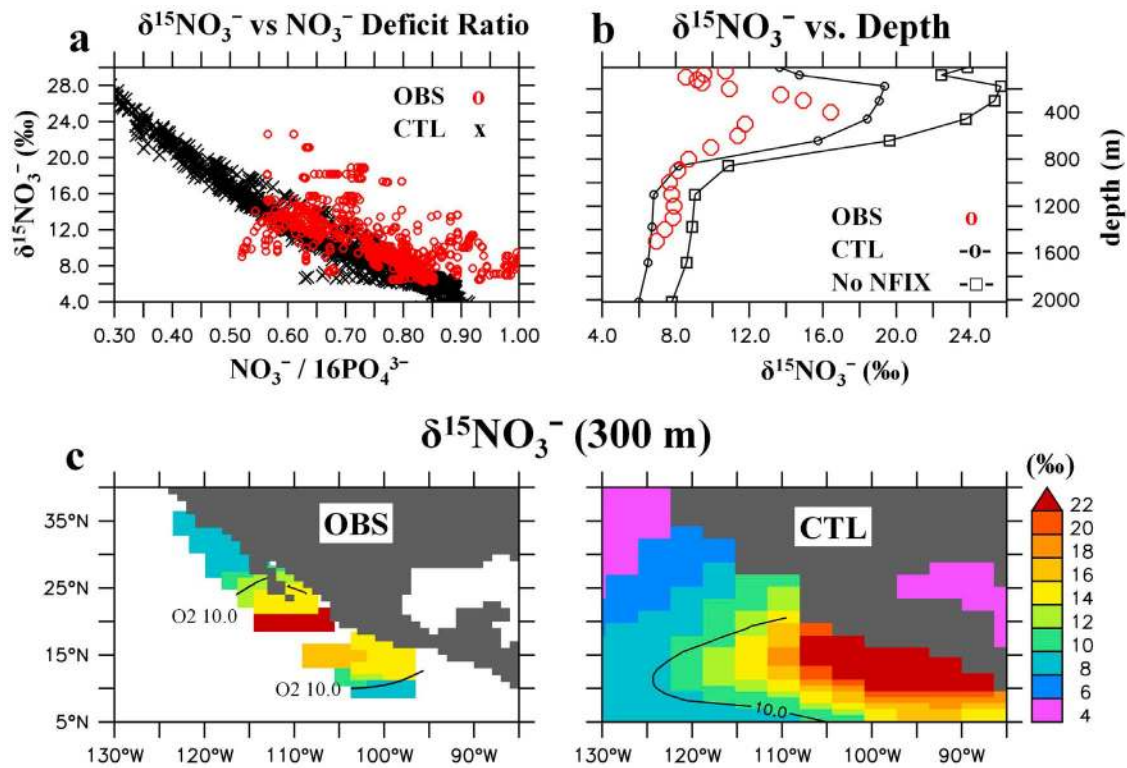


Figure 6. Comparison of the ETNP with the $\delta^{15}\text{NO}_3^-$ database and CTL: (a) $\delta^{15}\text{NO}_3^-$ versus $N' = \text{NO}_3^- - 16\text{PO}_4^{3-}$, (b) horizontally averaged (within $10 \mu\text{M O}_2$ contour) depth $\delta^{15}\text{NO}_3^-$ profiles including the experiment where the isotope effect of N_2 Fixation is neglected (no NFIX), and (c) subsurface $\delta^{15}\text{NO}_3^-$ with a $10 \mu\text{M O}_2$ contour line.

596 significant coastal upwelling (e.g., off Peru and NW
597 Mexico) (Figure S3), too large for water column denitri-
598 fication to occur. Preliminary experiments suggest that
599 increased vertical resolution can improve the simulation of
600 productivity and suboxia in the Eastern Tropical South
601 Pacific (not shown).

602 [29] The ability to reproduce the equatorial undercurrents
603 that transport relatively oxygen-rich water from the western
604 basin is also important for the simulation of the Eastern
605 Pacific suboxic zones. The anisotropic viscosity scheme
606 [Large et al., 2001] improves equatorial dynamics consid-
607 erably (Text S2 and Figure S1). The Pacific Equatorial
608 Undercurrent increases from 0.15 m/s to nearly 0.8 m/s, just
609 slightly weaker than observations, which show velocities
610 near 1 m/s (Figure S2). The North Equatorial Countercurrent
611 in the model also displays lower current velocities than
612 observed, and does not deliver enough oxygen-rich water
613 directly to the ETNP suboxic zone. This is likely the main
614 reason why the simulated suboxic zone is too large and
615 located too far south (by $\sim 5^\circ$) relative to observations
616 (Figure S3). This results in higher rates of water column
617 denitrification and higher $\delta^{15}\text{NO}_3^-$ values, as well as more N-
618 deficient water in the suboxic zone compared to observations
619 (Figure 6).

620 [30] Since the locally high $\delta^{15}\text{NO}_3^-$ values exist in too
621 small NO_3^- concentrations, when they transport out of the
622 denitrification zone and mix with water with much higher

NO_3^- , the high $\delta^{15}\text{NO}_3^-$ value is largely diluted away because
623 the resulting $\delta^{15}\text{NO}_3^-$ value is weighted toward the water
624 parcel with more NO_3^- . This “dilution effect” [Deutsch et al.,
625 2004] reduces the impact that water column denitrification
626 has on $\delta^{15}\text{NO}_3^-$ outside of denitrification zones, and thus
627 decreases its actual isotope effect on setting the global mean
628 $\delta^{15}\text{NO}_3^-$. This is the main reason why the model requires a
629 relatively low sedimentary to water column denitrification
630 ratio of 1:3 to set the global mean $\delta^{15}\text{NO}_3^-$ to 5‰ compared
631 to estimates from one-box models [Brandes and Devol,
632 2002; Altabet, 2007], which cannot account for any
633 important effects that occur locally within the denitrification
634 zone. However, note that our model significantly over-
635 estimates NO_3^- consumption via water column denitrifica-
636 tion in the ETNP compared to observations (Figure 6a).
637 Therefore, it is likely that our sedimentary to water
638 denitrification ratio of 1:3 is too low, but it does highlight
639 the importance that the NO_3^- consumption/dilution effect can
640 have on determining the global mean $\delta^{15}\text{NO}_3^-$.
641

[31] Figure 6 shows model $\delta^{15}\text{NO}_3^-$ compared to obser-
642 vational $\delta^{15}\text{NO}_3^-$ data collected during November 1999
643 [Sigman et al., 2005] and October 2000 (M. Altabet,
644 unpublished data, 2010). The model captures the general
645 observed trend of increasing $\delta^{15}\text{NO}_3^-$ as NO_3^- is consumed
646 during water column denitrification (Figure 6a). The model’s
647 too low N:P ratio for diazotrophs may partly explain its
648 incapacity to simulate some of the relatively high N' values
649

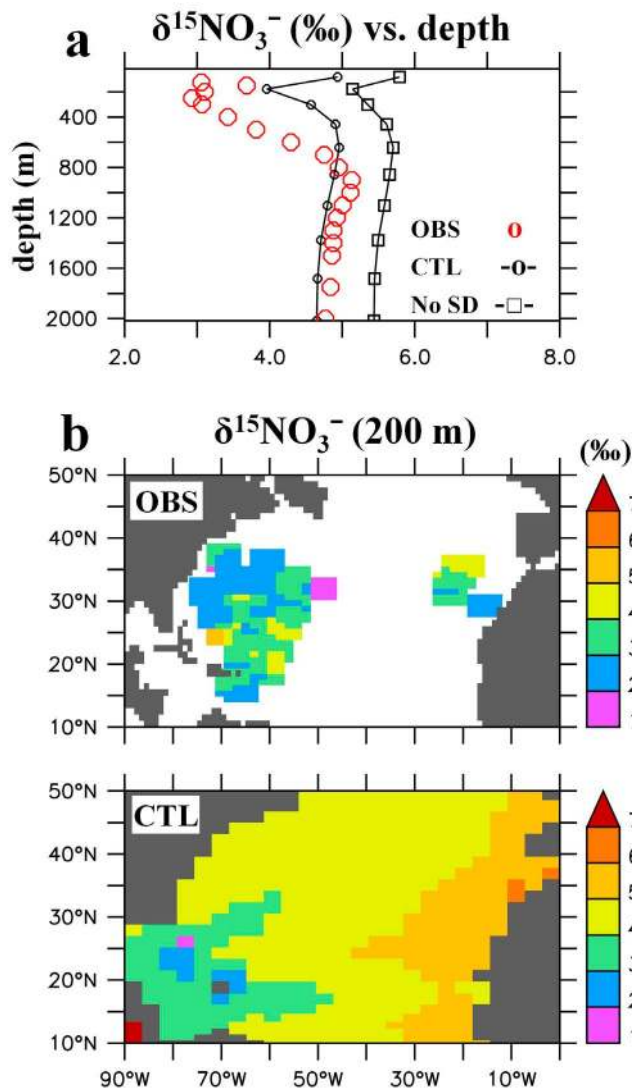


Figure 7. Comparison of the North Atlantic with the $\delta^{15}\text{NO}_3^-$ database and CTL. (a) Horizontally averaged (over available data) depth $\delta^{15}\text{NO}_3^-$ profiles including the experiment where sedimentary denitrification is neglected (no SD); (b) subsurface $\delta^{15}\text{NO}_3^-$.

650 of observations. The range of simulated values is also
 651 likely to be more limited compared to the observations due
 652 to the missing interannual and synoptic climate variability
 653 in the model. Figure 6b compares the horizontally aver-
 654 aged $\delta^{15}\text{NO}_3^-$ depth profiles only within the hypoxic zone
 655 ($\text{O}_2 < 10 \mu\text{M}$) at 300 m (contoured on Figure 6c) to
 656 account for the displaced OMZ. Within this region, the
 657 model is able to capture the general vertical distribution of
 658 $\delta^{15}\text{NO}_3^-$ seen in the measured data, such as the surface
 659 minimum and subsurface maximum.

660 [32] $\delta^{15}\text{NO}_3^-$ in the ETNP decreases toward the surface
 661 [Cline and Kaplan, 1975; Brandes et al., 1998; Voss et al.,
 662 2001; Sigman et al., 2005] suggesting a source of isotopi-
 663 cally light N at the surface. [Brandes et al., 1998] proposed
 664 that in the Arabian Sea as much as 30% of primary pro-

duction must be supported by N_2 fixation in order to account 665
 for the low surface $\delta^{15}\text{NO}_3^-$. Other observations also suggest 666
 that the decrease in $\delta^{15}\text{NO}_3^-$ toward the surface is likely due 667
 to the fixation of atmospheric N_2 and the subsequent, 668
 closely coupled remineralization-nitrification cycle [Sigman 669
 et al., 2005]. We test this hypothesis by comparing the 670
 observations with the model experiment in which the isotope 671
 effect of N_2 fixation is neglected (“No NFIX”). In this 672
 case, the model overestimates surface $\delta^{15}\text{NO}_3^-$ by ~12‰ 673
 (Figure 6b) and the surface minimum is not simulated. This 674
 experiment demonstrates that the input of isotopically light 675
 fixed N from N_2 fixation in the model best explains the 676
 decreasing trend of $\delta^{15}\text{NO}_3^-$ observations toward the surface. 677
 In the model, 20% of the fixed N loss via denitrification is 678
 reintroduced into the surface by N_2 fixation occurring 679
 directly above the denitrification zone in the ETNP. The fact 680
 that the difference between the subsurface maximum and the 681
 near surface minimum is underestimated in the model (6‰ 682
 versus 8‰ in the observations) suggests that in the real 683
 world the locally reintroduced fraction could be larger than 684
 20%. 685

4.3. North Atlantic 686

[33] Uncertainties regarding processes that can affect the 687
 nitrogen isotope signal make it challenging to interpret and 688
 simulate nitrogen isotopes in the North Atlantic. Estimates 689
 of atmospheric N deposition [Duce et al., 2008] and the 690
 assimilation-remineralization-nitrification cycle are not well 691
 constrained. Although atmospheric N deposition may be 692
 significant in this region [Michaels et al., 1996; Lipschultz 693
 et al., 2002; Knapp et al., 2005, 2008], its isotopic com- 694
 position is not well known and therefore is not included in 695
 the model at this time. Figure 7 shows the comparison of 696
 annual model $\delta^{15}\text{NO}_3^-$ with available observations from 697
 cruises in May 2001 and 2004 (M. Altabet and J. P. 698
 Montoya, unpublished data, 2010), October 2002 [Knapp 699
 et al., 2008], and May 2005 [Bourbonnais et al., 2009]. 700
 The model overestimates the $\delta^{15}\text{NO}_3^-$ values everywhere, 701
 by 0.9‰ on average and by 2‰ at 200 m depth, pre- 702
 sumably due mostly to the underestimation of N_2 fixation, 703
 but possibly also because atmospheric N deposition and/or 704
 fractionation during the remineralization of organic matter 705
 are not included. Both of these processes would act to 706
 decrease subsurface values of $\delta^{15}\text{NO}_3^-$. Underestimated N' 707
 in the North Atlantic (Figure S3) also indicates too little 708
 N_2 fixation, but we again note the too low N:P ratio for 709
 diazotrophs also contributes to this N' underestimation to 710
 some degree. 711

[34] N_2 fixation is most likely underestimated in the 712
 model because it does not consider dynamic elemental 713
 cycling of the microbial loop. It has been suggested that 714
 DOP is more labile relative to DON and recycles through 715
 the microbial loop more efficiently, which can help relieve 716
 diazotrophs of P limitation in this region [Wu et al., 2000] 717
 and enhance N_2 fixation. The model is able to reproduce the 718
 pattern of low $\delta^{15}\text{NO}_3^-$ in the thermocline qualitatively, just 719
 not quantitatively to the extent present in the observations. 720
 Sedimentary denitrification in the North Atlantic stimulates 721
 enough N_2 fixation in the model to generate a subsurface 722
 $\delta^{15}\text{NO}_3^-$ minimum. When sedimentary denitrification is 723

724 switched off (“No SD”), the thermocline minimum is not
725 simulated. This suggests that sedimentary denitrification is
726 an important factor influencing N_2 fixation in the Subtrop-
727 ical North Atlantic, but not the only factor.

728 5. Discussion and Conclusions

729 [35] A new model of nitrogen isotopes has been im-
730 plemented into the three-dimensional ocean component of a
731 global Earth system climate model capable of millennial
732 timescale simulations. Despite some model deficiencies, we
733 have shown that this model can successfully reproduce the
734 general spatial patterns of $\delta^{15}NO_3^-$ measured in the ocean.
735 Sensitivity experiments allowed us to isolate the individual
736 N isotope effects of various N transformational processes on
737 the global distribution of $\delta^{15}N$. Algal NO_3^- assimilation,
738 water column denitrification, and N_2 fixation all have strong
739 influences in setting the global patterns of $\delta^{15}NO_3^-$ in the
740 ocean, whereas the effect of zooplankton excretion is
741 weaker.

742 [36] These simulations show that the isotope effect of
743 algal NO_3^- assimilation can drive very large spatial gradients
744 in both $\delta^{15}NO_3^-$ and $\delta^{15}N$ OM depending on the ocean
745 environment (Figure 3). In HNLC areas where surface NO_3^-
746 utilization is low and algae are able to fractionate NO_3^- at
747 their designated enrichment factor, the $\delta^{15}N$ OM signature
748 decreases. However, when NO_3^- utilization is high, the $\delta^{15}N$
749 OM signature is more similar to the $\delta^{15}NO_3^-$ value it con-
750 sumes because the effective degree of fractionation becomes
751 much lower (see section 3.1). Surface NO_3^- utilization gra-
752 dients can transition rapidly, for example due to changes in
753 ocean circulation, and can possibly drive large and rapid
754 changes in $\delta^{15}NO_3^-$ and $\delta^{15}N$ OM. The important influence
755 of surface NO_3^- utilization on the global distribution of N
756 isotopes in the model suggests that changes in surface NO_3^-
757 utilization patterns throughout Earth’s history could con-
758 tribute to large fluctuations in $\delta^{15}N$ observed in sediment
759 records, especially near fronts where large surface NO_3^-
760 gradients exist [see also *Altabet and Francois*, 1994; *Farrell*
761 *et al.*, 1995; *Sigman et al.*, 1999; *Brunelle et al.*, 2007;
762 *Galbraith et al.*, 2008; *Robinson and Sigman*, 2008].

763 [37] The model simulates a strong direct and indirect
764 isotope effect of denitrification. High $\delta^{15}NO_3^-$ produced by
765 water column denitrification has clear regional impacts and
766 is also responsible for overall elevated $\delta^{15}NO_3^-$ of the ocean
767 relative to the N_2 fixation source (see below). The indirect
768 effect of both water column and sediment denitrification is
769 mediated by the production of N-deficient water, which
770 creates an ecological niche for diazotrophs. This stimulates
771 additional N_2 fixation when other suitable conditions for N_2
772 fixation also exist (e.g., warm ($>20^\circ C$), N-depleted water
773 with sufficient P and Fe). This indirect effect also attenuates
774 the horizontal circulation of high $\delta^{15}NO_3^-$ waters, originating
775 from regions of water column denitrification, which causes
776 its direct isotope effect to be regionalized to suboxic zones
777 in the model.

778 [38] Key features of the model have been identified that
779 are in need of further development. The coarse resolution
780 physical circulation model does not fully resolve the
781 dynamics of coastal upwelling regimes, which in part drive

the flux of organic matter toward the seafloor sediments and 782
its remineralization in the water column, as well as indi- 783
rectly influences ventilation of suboxic zones. This is critical 784
in the simulation of water column denitrification and sedi- 785
mentary denitrification, which are important processes with 786
respect to the global N isotope balance. Future model ver- 787
sions will include additional vertical levels to better resolve 788
continental shelves as well as higher horizontal resolution. 789
The model neglects dynamic elemental stoichiometry such 790
as high N:P ratios of diazotrophs and the more efficient 791
recycling of DOP relative to DON in microbial loops, which 792
can help relieve diazotrophs of their P limitation and allow 793
them to fix additional N_2 into the oceanic fixed N pool in 794
oligotrophic waters. The ecosystem model also suffers from 795
the exclusion of Fe as a prognostic tracer preventing it from 796
being able to simulate differences in ecosystems limited by 797
marconutrients (NO_3^- , PO_4^{3-}) versus micronutrients (Fe). 798

[39] Future applications of this model will include simu- 799
lations of past climates, and direct comparison with $\delta^{15}N$ 800
sediment records will be used to test the model results. This 801
approach may be a useful to quantify past interactions 802
between the marine N cycle and its isotopes, as well as their 803
impact on climate and may provide new insights into 804
important physical and biogeochemical changes throughout 805
Earth’s history. 806

Appendix A: Nitrogen Isotope Model 807

[40] The open system fractionation equation is used for 808
fractionation during algal NO_3^- assimilation [*Altabet and* 809
Francois, 2001]: 810

$$\delta^{15}P_0 = \delta^{15}NO_3^- - \epsilon_{ASSIM}(1 - u_{NO_3}), \quad (A1)$$

where $\delta^{15}P_0$ is the $\delta^{15}N$ of phytoplankton biomass assim- 811
lated during one time step, Δt , and u_{NO_3} is the fraction of 812
 NO_3^- available that is converted into biomass ($u_{ASSIM} =$ 813
 $J_O P_O \times \Delta t / NO_3^-$). When algae assimilate all available NO_3^- 814
into their biomass (i.e., $u_{ASSIM} = 1$) they will incorporate the 815
same $\delta^{15}N$ value as that of the source material. Many studies 816
have estimated the fractionation factor in both laboratory 817
and ocean environments. A wide variety of values have been 818
reported in culture settings ranging from 0.7‰ to 23‰ 819
[*Wada and Hattori*, 1978; *Montoya and McCarthy*, 1995; 820
Waser et al., 1998; *Needoba et al.*, 2003; *Granger et al.*, 821
2004]. A more confined range has been observed in field 822
estimates from 4‰ to 15‰ [*Wada*, 1980; *Altabet et al.*, 823
1991, 1999b; *Sigman et al.*, 1999; *Altabet and Francois*, 824
2001; *Karsh et al.*, 2003; *DiFiore et al.*, 2006]. In our 825
model we choose a constant value of 5‰ which is near the 826
majority of estimates, although it is important to bear in 827
mind the uncertainty in the parameter choice and the possi- 828
bility that it varies in space and time. 829

[41] Nitrate in suboxic waters have been observed to have 830
much higher $\delta^{15}N$ values due to fractionation during deni- 831
trification. Observations from present-day suboxic zones in 832
the Eastern Tropical North Pacific (ETNP) and the Arabian 833
Sea (AS) have reported fractionation factors ranging from 834
22 to 30‰ [*Cline and Kaplan*, 1975; *Liu and Kaplan*, 1989; 835
Brandes et al., 1998; *Altabet et al.*, 1999b; *Voss et al.*, 836

837 2001]; we adopt a value of 25‰ in the model. Note that
838 because these estimates were derived from field studies in
839 which the isotope effect was estimated from the total
840 nitrogen loss, they implicitly include the effect of anammox
841 [Galbraith *et al.*, 2008]. Fractionation during denitrification
842 is also simulated using the open system fractionation
equation

$$\delta^{15}\text{NO}_3^{\text{OX}} = \delta^{15}\text{NO}_3^- - \varepsilon_{\text{WCD}}(1 - u_{\text{NO}_3}), \quad (\text{A2})$$

843 where NO_3^{OX} is the oxygen-equivalent reduction of nitrate
844 converted into N_2 gas during denitrification. The term u_{DENI}
845 is the fraction of available NO_3^- which is reduced into N_2 gas
846 ($u_{\text{NO}_3} = \mu_{\text{D}}D \times 0.8 \times R_{\text{O:N}} \times r_{\text{sox}}^{\text{NO}_3} \times L_{\text{NO}_3} \times \Delta t/\text{NO}_3$).
847 [42] Excretion is the process responsible for the step-
848 wise enrichment of $\delta^{15}\text{N}$ along the trophic chain in our
849 model and is simulated using the instantaneous fraction-
850 ation equation:

$$\delta^{15}\text{NO}_3^- = \delta^{15}\text{Z} - \varepsilon_{\text{EXCR}}. \quad (\text{A3})$$

851 The instantaneous fractionation equation is used because
852 excretion will always be a small fraction of the total
853 zooplankton biomass and has been measured to be
854 depleted by $\sim 6\%$ relative to its body [Montoya, 2008],
855 which is the source of the excreted nitrogen. This leads to
856 the average enrichment of ~ 3.4 per trophic level
857 [Minagawa and Wada, 1984].

858 [43] Implementing these fractionation equations into the
859 marine ecosystem model requires us to consider the ex-
860 changes of ^{14}N and ^{15}N between the various N pools sep-
861 arately. Total nitrogen abundance now has the form

$$\text{N} = {}^{14}\text{N} + {}^{15}\text{N} \quad (\text{A4})$$

862 for each variable in the isotope model. A fractionation
863 coefficient is calculated for each process so the same
864 equations for total N can be applied to ^{15}N [Giraud *et al.*,
865 2000]. For example, consider fractionation during algal
866 NO_3^- assimilation. The isotopic ratio of new nitrogen bio-
867 mass (P_{O}) is found using equations (1) and (2):

$${}^{15}P_{\text{O}} = \beta_{\text{ASSIM}} {}^{14}P_{\text{O}} \quad (\text{A5})$$

868 where

$$\beta_{\text{ASSIM}} = \frac{{}^{15}\text{NO}_3}{{}^{14}\text{NO}_3} - \frac{\varepsilon_{\text{ASSIM}}(1 - u_{\text{NO}_3})R_{\text{std}}}{1000}. \quad (\text{A6})$$

869 [44] Applying equations (S4) and (S5) in Text S2 gives
870 the amount of new ${}^{15}P_{\text{O}}$ relative to the amount of total new
871 nitrogen biomass, which is given by the primary production
872 ($J_{\text{O}}P_{\text{O}}$), calculated by the marine ecosystem model:

$${}^{15}P_{\text{O}} = \frac{\beta_{\text{ASSIM}}}{1 + \beta_{\text{ASSIM}}} J_{\text{O}}P_{\text{O}}. \quad (\text{A7})$$

873 Analogous derivations can be done for all fractionation
874 coefficients. The time-dependent set of equations for ^{15}N

which are embedded into the marine ecosystem model are as
875 follows:

$$\begin{aligned} \frac{\partial {}^{15}\text{NO}_3}{\partial t} = & \left(R_{\text{D}}\mu_{\text{D}}D + \frac{\beta_{\text{EXCR}}}{1 + \beta_{\text{EXCR}}}\gamma_2Z + R_{\text{P}}\mu_{\text{P}}P_{\text{O}} \right. \\ & \left. - \frac{\beta_{\text{ASSIM}}}{1 + \beta_{\text{ASSIM}}}J_{\text{O}}P_{\text{O}} - \frac{\beta_{\text{ASSIM}}}{1 + \beta_{\text{ASSIM}}}u_{\text{N}}J_{\text{D}}P_{\text{D}} \right) \\ & \times \left[1 - \frac{\beta_{\text{WCD}}}{1 + \beta_{\text{WCD}}}0.8R_{\text{O:N}}r_{\text{sox}}^{\text{NO}_3}L_{\text{NO}_3} \right], \quad (\text{A8}) \end{aligned}$$

876

$$\frac{\partial {}^{15}P_{\text{O}}}{\partial t} = \frac{\beta_{\text{ASSIM}}}{1 + \beta_{\text{ASSIM}}}J_{\text{O}}P_{\text{O}} - R_{\text{P}}\mu_{\text{P}}P_{\text{O}} - R_{\text{P}_\text{O}}G(P_{\text{O}})Z - R_{\text{P}_\text{O}}\mu_{\text{P}_2}P_{\text{O}}^2, \quad (\text{A9})$$

877

$$\begin{aligned} \frac{\partial {}^{15}P_{\text{D}}}{\partial t} = & \left(\frac{\beta_{\text{ASSIM}}}{1 + \beta_{\text{ASSIM}}}u_{\text{N}} + \frac{\beta_{\text{NFIX}}}{1 + \beta_{\text{NFIX}}}(1 - u_{\text{N}}) \right) J_{\text{D}}P_{\text{D}} \\ & + -R_{\text{P}_\text{D}}G(P_{\text{D}})Z - R_{\text{P}_\text{D}}\mu_{\text{P}}P_{\text{D}}, \quad (\text{A10}) \end{aligned}$$

878

$$\frac{\partial {}^{15}Z}{\partial t} = \gamma_1[R_{\text{P}_\text{O}}G(P_{\text{O}}) + R_{\text{P}_\text{D}}G(P_{\text{D}})]Z - \frac{\beta_{\text{EXCR}}}{1 + \beta_{\text{EXCR}}}\gamma_2Z - R_{\text{Z}}\mu_{\text{Z}}Z^2, \quad (\text{A11})$$

879

$$\begin{aligned} \frac{\partial {}^{15}D}{\partial t} = & (1 - \gamma_1)[R_{\text{P}_\text{O}}GP_{\text{O}} + R_{\text{P}_\text{D}}GP_{\text{D}}]Z + R_{\text{P}_\text{D}}\mu_{\text{P}}P_{\text{D}} + R_{\text{P}_\text{O}}\mu_{\text{P}_2}P_{\text{O}}^2 \\ & + R_{\text{Z}}\mu_{\text{Z}}Z^2 - R_{\text{D}}\mu_{\text{D}}D - R_{\text{D}}\omega_{\text{D}}\frac{\partial D}{\partial z}, \quad (\text{A12}) \end{aligned}$$

where $R_{\text{N}} = P_{\text{O}}, P_{\text{D}}, Z, D = {}^{15}\text{N}/({}^{14}\text{N} + {}^{15}\text{N})$ is the ratio of
880 heavy over total nitrogen. The complete parameter
881 description is provided in Text S2. Here it suffices to note
882 that the equations for total nitrogen (${}^{14}\text{N} + {}^{15}\text{N}$) are identical
883 to the ones of ${}^{15}\text{N}$ except that $R_{\text{X}} = \beta_{\text{X}}/(1 + \beta_{\text{X}}) = 1$ in the
884 total nitrogen equations.
885

[45] The model was carefully tested with zero fraction-
886 ation in order to quantify and minimize numerical errors,
887 which can occur for example due to slightly negative val-
888 ues of biological tracers caused by inaccuracies of the
889 advection scheme. The biological code was adjusted to
890 avoid negative concentrations as much as possible. Initially
891 numerical errors in $\delta^{15}\text{N}$ ranged from $\pm 1\%$ in grid points
892 at the seafloor to $\pm 0.1\%$ in the upper ocean. Setting $R_{\text{std}} =$
893 1 instead of $R_{\text{std}} = 0.0036765$, the actual atmospheric N_2
894 isotope ratio, reduces the numerical errors by over an order
895 of magnitude. R_{std} is set to the value 1 so both isotope
896 variables will be on the same order of magnitude. This
897 prevents ${}^{15}\text{N}$ from becoming very close to zero as often,
898 where inaccuracies of the advection scheme can cause it to
899 be negative. This modification amounts to a scaling of ${}^{15}\text{N}$
900 and ${}^{14}\text{N}$ by a constant factor which does not affect the
901 $\delta^{15}\text{N}$ dynamics. The remaining numerical errors of $\pm 0.1\%$
902 in the deep ocean and $\pm 0.01\%$ in the upper ocean are 2
903

904 orders of magnitude smaller than the observed variability.
 905 The model is integrated for over 5,000 years as it approaches
 906 equilibrium.

907 [46] **Acknowledgments.** We would like to thank Daniel Sigman,
 908 Angela Knapp, and Peter DiFiore for contributing data to this study. Reviews
 909 by two anonymous referees were appreciated. This work is funded by the
 910 Marine Geology and Geophysics program of the National Science Founda-
 911 tion (grant 0728315-OCE).

912 References

- 913 Altabet, M. A. (2007), Constraints on oceanic N balance/imbalance
 914 from sedimentary ^{15}N records, *Biogeosciences*, 4, 75–86, doi:10.5194/
 915 bg-4-75-2007.
- 916 Altabet, M. A., and R. Francois (1994), Sedimentary nitrogen isotopic ratio
 917 as a recorder for surface ocean nitrate utilization, *Global Biogeochem.*
 918 *Cycles*, 8(1), 103–116, doi:10.1029/93GB03396.
- 919 Altabet, M. A., and R. Francois (2001), Nitrogen isotope biogeochemistry
 920 of the Antarctic Polar Frontal Zone at 170W, *Deep Sea Res., Part II*, 48
 921 (19–20), 4247–4273, doi:10.1016/S0967-0645(01)00088-1.
- 922 Altabet, M. A., W. G. Deuser, S. Honjo, and C. Stienen (1991), Seasonal
 923 and depth-related changes in the source of sinking particles in the North
 924 Atlantic, *Nature*, 354, 136–139, doi:10.1038/354136a0.
- 925 Altabet, M. A., D. W. Murray, and W. L. Prell (1999a), Climatically linked
 926 oscillations in Arabian Sea denitrification over the past 1 m.y.: Implica-
 927 tions for the marine N cycle, *Paleoceanography*, 14(6), 732–743,
 928 doi:10.1029/1999PA900035.
- 929 Altabet, M. A., C. Pilskan, R. Thunell, C. Pride, D. Sigman, F. Chavez, and
 930 R. Francois (1999b), The nitrogen isotope biogeochemistry of sinking
 931 particles from the margin of the eastern North Pacific, *Deep Sea Res.,*
 932 *Part I*, 46, 655–679, doi:10.1016/S0967-0637(98)00084-3.
- 933 Bourbonnais, A., M. F. Lehmann, J. J. Wanick, and D. E. Schulz-Bull
 934 (2009), Nitrate isotope anomalies reflect N_2 fixation in the Azores Front
 935 region (subtropical NE Atlantic), *J. Geophys. Res.*, 114, C03003,
 936 doi:10.1029/2007JC004617.
- 937 Brandes, J. A., and A. H. Devol (1997), Isotopic fractionation of oxygen
 938 and nitrogen in coastal marine sediments, *Geochim. Cosmochim. Acta*,
 939 61(9), 1793–1801, doi:10.1016/S0016-7037(97)00041-0.
- 940 Brandes, J. A., and A. H. Devol (2002), A global marine-fixed nitrogen
 941 isotopic budget: Implications for Holocene nitrogen cycling, *Global*
 942 *Biogeochem. Cycles*, 16(4), 1120, doi:10.1029/2001GB001856.
- 943 Brandes, J. A., A. H. Devol, T. Yoshinari, D. A. Jayakumar, and S. W. A.
 944 Naqvi (1998), Isotopic composition of nitrate in the central Arabian
 945 Sea and eastern tropical North Pacific: A tracer for mixing and nitro-
 946 gen cycles, *Limnol. Oceanogr.*, 43(7), 1680–1689, doi:10.4319/
 947 lo.1998.43.7.1680.
- 948 Brunelle, B. G., D. M. Sigman, M. S. Cook, L. D. Keigwin, G. H. Haug,
 949 B. Plessen, G. Schettler, and S. L. Jaccard (2007), Evidence from diatom-
 950 bound nitrogen isotopes for subarctic Pacific stratification during the last
 951 ice age and a link to North Pacific denitrification changes, *Paleoceanogra-*
 952 *phy*, 22, PA1215, doi:10.1029/2005PA001205.
- 953 Carpenter, E. J., and D. G. Capone (2008), Nitrogen fixation in the marine
 954 environment, in *Nitrogen in the Marine Environment*, edited by D. G.
 955 Capone et al., pp. 141–198, Elsevier, New York, doi:10.1016/B978-0-
 956 12-372522-6.00004-9.
- 957 Carpenter, E. J., H. R. Harvey, B. Fry, and D. G. Capone (1997), Biogeo-
 958 chemical tracers of the marine cyanobacterium *Trichodesmium*, *Deep Sea*
 959 *Res., Part I*, 44(1), 27–38, doi:10.1016/S0967-0637(96)00091-X.
- 960 Church, M. J., K. M. Bjorkman, D. M. Karl, M. A. Saito, and J. P. Zehr
 961 (2008), Regional distributions of nitrogen-fixing bacteria in the Pacific
 962 Ocean, *Limnol. Oceanogr.*, 53(1), 63–77.
- 963 Cline, J. D., and I. R. Kaplan (1975), Isotopic fractionation of dissolved
 964 nitrate during denitrification in the eastern tropical North Pacific Ocean,
 965 *Mar. Chem.*, 3(4), 271–299, doi:10.1016/0304-4203(75)90009-2.
- 966 Codispoti, L. A. (2007), An oceanic fixed nitrogen sink exceeding
 967 400 Tg N a⁻¹ vs the concept of homeostasis in the fixed-nitrogen inven-
 968 tory, *Biogeosciences*, 4, 233–253, doi:10.5194/bg-4-233-2007.
- 969 Codispoti, L. A., and F. A. Richards (1976), An analysis of the horizontal
 970 regime of denitrification in the eastern tropical North Pacific, *Limnol.*
 971 *Oceanogr.*, 21(3), 379–388, doi:10.4319/lo.1976.21.3.0379.
- 972 Delwiche, C. C., and P. L. Steyn (1970), Nitrogen isotope fractionation in
 973 soils and microbial reactions, *Environ. Sci. Technol.*, 4, 929–935,
 974 doi:10.1021/es60046a004.
- Deutsch, C., D. M. Sigman, R. C. Thunell, A. N. Meckler, and G. H. Haug 975
 (2004), Isotopic constraints on glacial/interglacial changes in the oceanic 976
 nitrogen budget, *Global Biogeochem. Cycles*, 18, GB4012, doi:10.1029/ 977
 2003GB002189. 978
- Deutsch, C., J. L. Sarmiento, D. M. Sigman, N. Gruber, and J. P. Dunne 979
 (2007), Spatial coupling of nitrogen inputs and losses in the ocean, 980
Nature, 445, 163–167, doi:10.1038/nature05392. 981
- DiFiore, P. J., D. M. Sigman, T. W. Trull, M. J. Lourey, K. Karsh, G. Cane, 982
 and R. Ho (2006), Nitrogen isotope constraints on subantarctic biogeo- 983
 chemistry, *J. Geophys. Res.*, 111, C08016, doi:10.1029/2005JC003216. 984
- Duce, R. A., et al. (2008), Impacts of atmospheric anthropogenic nitro- 985
 gen on the open ocean, *Science*, 320(5878), 893–897, doi:10.1126/ 986
 science.1150369. 987
- Falkowski, P. G. (1997), Evolution of the nitrogen cycle and its influ- 988
 ence on the biological sequestration of CO₂ in the ocean, *Nature*, 989
 387, 272–275, doi:10.1038/387272a0. 990
- Farrell, J. W., T. F. Pedersen, S. E. Calvert, and B. Nielsen (1995), Glacial- 991
 interglacial changes in nutrient utilization in the equatorial Pacific Ocean, 992
Nature, 377, 514–517, doi:10.1038/377514a0. 993
- Galbraith, E. G. (2006), Interactions between climate and the marine nitro- 994
 gen cycle on glacial-interglacial timescales, Ph.D. thesis, Univ. of British 995
 Columbia, Vancouver. 996
- Galbraith, E. G., M. Kienast, T. F. Pedersen, and S. E. Calvert (2004), 997
 Glacial-interglacial modulation of the marine nitrogen cycle by high- 998
 latitude O₂ supply to the global thermocline, *Paleoceanography*, 19, 999
 PA4007, doi:10.1029/2003PA001000. 1000
- Galbraith, E. G., M. Kienast, S. L. Jaccard, T. F. Pedersen, B. G. Brunelle, 1001
 D. M. Sigman, and T. Kiefer (2008), Consistent relationship between 1002
 global climate and surface nitrate utilization in the western subarctic 1003
 Pacific throughout the last 500 ka, *Paleoceanography*, 23, PA2212, 1004
 doi:10.1029/2007PA001518. 1005
- Gent, P. R., and J. C. McWilliams (1990), Isopycnal mixing in ocean 1006
 circulation models, *J. Phys. Oceanogr.*, 20, 150–155, doi:10.1175/ 1007
 1520-0485(1990)020<0150:IMOCM>2.0.CO;2. 1008
- Giraud, X., P. Bertrand, V. Garçon, and I. Dadou (2000), Modeling d¹⁵N 1009
 evolution: First paleoceanographic applications in a coastal upwelling 1010
 system, *J. Mar. Res.*, 58(4), 609–630, doi:10.1357/002224000321511043. 1011
- Granger, J., D. M. Sigman, J. A. Needoba, and P. J. Harrison (2004), Cou- 1012
 pled nitrogen and oxygen isotope fractionation of nitrate during assimila- 1013
 tion by cultures of marine phytoplankton, *Limnol. Oceanogr.*, 49(5), 1014
 1763–1773, doi:10.4319/lo.2004.49.5.1763. 1015
- Holl, C. M., and J. P. Montoya (2005), Interactions between nitrate uptake 1016
 and nitrogen fixation in continuous cultures of the marine diazotroph *Tri-* 1017
chodesmium (cyanobacteria), *J. Phycol.*, 41, 1178–1183, doi:10.1111/ 1018
 j.1529-8817.2005.00146.x. 1019
- Karl, D., A. Michaels, B. Bergman, D. Capone, E. Carpenter, R. Letelier, 1020
 F. Lipschultz, H. Paerl, D. Sigman, and L. Stal (2002), Dinitrogen fixation 1021
 in the world's oceans, *Biogeochemistry*, 57–58(1), 47–98, doi:10.1023/ 1022
 A:1015798105851. 1023
- Karsh, K. L., T. W. Trull, M. J. Lourey, and D. M. Sigman (2003), Relation- 1024
 ship of nitrogen isotope fractionation to phytoplankton size and iron avail- 1025
 ability during the Southern Ocean Iron RElease Experiment (SOIREE), 1026
Limnol. Oceanogr., 48(3), 1058–1068, doi:10.4319/lo.2003.48.3.1058. 1027
- Kienast, S. S., S. E. Calvert, and T. F. Pedersen (2002), Nitrogen isotope 1028
 productivity variations along the northeast Pacific margin over the last 1029
 120 kyr: Surface and subsurface paleoceanography, *Paleoceanography*, 1030
 17(4), 1055, doi:10.1029/2001PA000650. 1031
- Kitajima, S., K. Furuya, F. Hashihama, S. Takeda, and J. Kanda (2009), 1032
 Latitudinal distribution of diazotrophs and their nitrogen fixation in 1033
 the tropical and subtropical western North Pacific, *Limnol. Oceanogr.*, 1034
 54(2), 537–547. 1035
- Knapp, A. N., D. M. Sigman, and F. Lipschultz (2005), N isotopic compo- 1036
 sition of dissolved organic nitrogen and nitrate at the Bermuda Atlantic 1037
 Time-series Study site, *Global Biogeochem. Cycles*, 19, GB1018, 1038
 doi:10.1029/2004GB002320. 1039
- Knapp, A. N., P. J. DiFiore, C. Deutsch, D. M. Sigman, and F. Lipschultz 1040
 (2008), Nitrate isotopic composition between Bermuda and Puerto Rico: 1041
 Implications for N₂ fixation in the Atlantic Ocean, *Global Biogeochem.* 1042
Cycles, 22, GB3014, doi:10.1029/2007GB003107. 1043
- Kuypers, M. M. M., A. O. Sliemers, G. Lavik, M. Schmid, B. B. Jorgensen, 1044
 J. G. Kuenen, J. S. S. Damste, M. Strous, and M. S. M. Jetten (2003), 1045
 Anaerobic ammonium oxidation by anammox bacteria in the Black 1046
 Sea, *Nature*, 422, 608–611, doi:10.1038/nature01472. 1047
- Kuypers, M. M. M., G. Lavik, D. Woebken, M. Schmid, B. M. Bernhard, 1048
 R. Amann, B. B. Jorgensen, and M. S. M. Jetten (2005), Massive nitro- 1049
 gen loss from the Benguela upwelling system through anaerobic ammo- 1050

- 1051 nium oxidation, *Proc. Natl. Acad. Sci. U. S. A.*, 102(18), 6478–6483, 1052 doi:10.1073/pnas.0502088102.
- 1053 Lam, P., G. Lavik, M. M. Jensen, J. van de Vossenberg, M. Schmid, 1054 D. Woebken, D. Gutierrez, M. S. M. Jetten, and M. M. M. Kuypers 1055 (2009), Revising the nitrogen cycle in the Peruvian oxygen minimum 1056 zone, *Proc. Natl. Acad. Sci. U. S. A.*, 106(12), 4752–4757, 1057 doi:10.1073/pnas.0812444106.
- 1058 Large, W. G., G. Danabasoglu, J. C. McWilliams, P. R. Gent, and F. O. 1059 Bryan (2001), Equatorial circulation of a global ocean climate model 1060 with anisotropic horizontal viscosity, *J. Phys. Oceanogr.*, 31, 518–536, 1061 doi:10.1175/1520-0485(2001)031<0518:ECOAGO>2.0.CO;2.
- 1062 Lehmann, M. F., D. M. Sigman, and W. M. Berelson (2004), Coupling the 1063 $^{15}\text{N}/^{14}\text{N}$ and $^{18}\text{O}/^{16}\text{O}$ of nitrate as a constraint on benthic nitrogen 1064 cycling, *Mar. Chem.*, 88, 1–20, doi:10.1016/j.marchem.2004.02.001.
- 1065 Lehmann, M. F., D. M. Sigman, D. C. McCorkle, B. G. Brunelle, 1066 S. Hoffmann, M. Kienast, G. Cane, and J. Clement (2005), Origin of 1067 the deep Bering Sea nitrate deficit: Constraints from the nitrogen and 1068 oxygen isotopic composition of water column nitrate and benthic nitrate 1069 fluxes, *Global Biogeochem. Cycles*, 19, GB4005, doi:10.1029/ 1070 2005GB002508.
- 1071 Lehmann, M. F., D. M. Sigman, D. C. McCorkle, J. Granger, S. Hoffmann, 1072 G. Cane, and B. G. Brunelle (2007), The distribution of nitrate 1073 $^{15}\text{N}/^{14}\text{N}$ in marine sediments and the impact of benthic nitrogen loss 1074 on the isotopic composition of oceanic nitrate, *Geochim. Cosmochim. 1075 Acta*, 71, 5384–5404, doi:10.1016/j.gca.2007.07.025.
- 1076 Letelier, R. M., and D. M. Karl (1996), Role of Trichodesmium spp. in the 1077 productivity of the subtropical North Pacific Ocean, *Mar. Ecol. Prog. 1078 Ser.*, 133, 263–273, doi:10.3354/meps133263.
- 1079 Letelier, R. M., and D. M. Karl (1998), *Trichodesmium* spp. physiology 1080 and nutrient fluxes in the North Pacific subtropical gyre, *Aquat. Microb. 1081 Ecol.*, 15, 265–276, doi:10.3354/ame015265.
- 1082 Lipschultz, F., N. R. Bates, C. A. Carlson, and D. A. Hansell (2002), New 1083 production in the Sargasso Sea: History and current status, *Global Bio- 1084 geochem. Cycles*, 16(1), 1001, doi:10.1029/2000GB001319.
- 1085 Liu, K.-K., and I. R. Kaplan (1989), The eastern tropical Pacific as a source 1086 of ^{15}N -enriched nitrate in seawater off southern California, *Limnol. 1087 Oceanogr.*, 34(5), 820–830, doi:10.4319/lo.1989.34.5.0820.
- 1088 Macko, S. A., M. L. Fogel, P. E. Hare, and T. C. Hoering (1987), Isotope 1089 fractionation of nitrogen and carbon in the synthesis of amino acids by 1090 microorganisms, *Chem. Geol. Isot. Geosci. Sect.*, 65(1), 79–92, 1091 doi:10.1016/0168-9622(87)90064-9.
- 1092 Mahowald, N. M., A. R. Baker, G. Bergametti, N. Brooks, R. A. Duce, 1093 T. D. Jickells, N. Kubilay, J. M. Prospero, and I. Tegen (2005), Atmo- 1094 spheric global dust cycle and iron inputs to the ocean, *Global Biogeo- 1095 chem. Cycles*, 19, GB4025, doi:10.1029/2004GB002402.
- 1096 Mariotti, A., J. C. Germon, P. Hubert, P. Kaiser, R. Letolle, A. Tardieux, 1097 and P. Tardieux (1981), Experimental determination of nitrogen kinetic 1098 isotope fractionation: Some principles; illustration for the denitrification 1099 and nitrification processes, *Plant Soil*, 62(3), 413–430, doi:10.1007/ 1100 BF02374138.
- 1101 McElroy, M. B. (1983), Marine biological controls on atmospheric CO_2 1102 and climate, *Nature*, 302, 328–329, doi:10.1038/302328a0.
- 1103 Michaels, A. F., D. Olson, J. L. Sarmiento, J. W. Ammerman, K. Fanning, 1104 R. Jahne, A. H. Knapp, F. Lipschultz, and J. M. Prospero (1996), Inputs, 1105 losses and transformations of nitrogen and phosphorus in the pelagic 1106 North Atlantic Ocean, in *Nitrogen Cycling in the North Atlantic Ocean 1107 and its Watersheds*, edited by R. W. Howarth, pp. 181–226, Kluwer 1108 Acad., Boston.
- 1109 Middelburg, J. J., K. Soetaert, P. M. J. Herman, and C. H. R. Heip (1996), 1110 Denitrification in marine sediments: A model study, *Global Biogeochem. 1111 Cycles*, 10(4), 661–673, doi:10.1029/96GB02562.
- 1112 Minagawa, M., and E. Wada (1984), Stepwise enrichment of ^{15}N along 1113 food chains: Further evidence and the relation between d^{15}N and animal 1114 age, *Geochim. Cosmochim. Acta*, 48(5), 1135–1140, doi:10.1016/0016- 1115 7037(84)90204-7.
- 1116 Minagawa, M., and E. Wada (1986), Nitrogen isotope ratios of red tide or- 1117 ganisms in the East China Sea: A characterization of biological nitrogen 1118 fixation, *Mar. Chem.*, 19(3), 245–259, doi:10.1016/0304-4203(86) 1119 90026-5.
- 1120 Montoya, J. P. (2008), Nitrogen stable isotopes in marine environments, 1121 in *Nitrogen in the Marine Environment*, edited by D. G. Capone et al., 1122 pp. 1277–1302, Elsevier, New York, doi:10.1016/B978-0-12-372522- 1123 6.00029-3.
- 1124 Montoya, J. P., and J. J. McCarthy (1995), Isotopic fractionation during 1125 nitrate uptake by phytoplankton grown in continuous culture, *J. Plankton 1126 Res.*, 17(3), 439–464, doi:10.1093/plankt/17.3.439.
- Montoya, J. P., C. M. Holl, J. P. Zehr, A. Hansen, T. A. Villareal, and D. G. 1127 Capone (2004), High rates of N_2 fixation by unicellular diazotrophs in 1128 the oligotrophic Pacific Ocean, *Nature*, 430, 1027–1032, doi:10.1038/ 1129 nature02824.
- Moore, J. K., and S. C. Doney (2007), Iron availability limits the ocean 1130 nitrogen inventory stabilizing feedbacks between marine denitrification 1131 and nitrogen fixation, *Global Biogeochem. Cycles*, 21, GB2001, 1132 doi:10.1029/2006GB002762.
- Mulder, A., A. A. van de Graaf, L. A. Robertson, and J. G. Kuenen (1995), 1133 Anaerobic ammonium oxidation discovered in a denitrifying fluidized 1134 bed reactor, *FEMS Microbiol. Ecol.*, 16(3), 177–184, doi:10.1111/ 1135 j.1574-6941.1995.tb00281.x.
- Naqvi, S. W. A. (2008), The Indian Ocean, in *Nitrogen in the Marine 1136 Environment*, edited by D. G. Capone et al., pp. 631–681, Elsevier, 1137 New York, doi:10.1016/B978-0-12-372522-6.00014-1.
- Needoba, J. A., N. A. Waser, P. J. Harrison, and S. E. Calvert (2003), 1138 Nitrogen isotope fractionation in 12 species of marine phytoplankton dur- 1139 ing growth on nitrate, *Mar. Ecol. Prog. Ser.*, 255, 81–91, doi:10.3354/ 1140 meps255081.
- Needoba, J. A., R. A. Foster, C. Sakamoto, J. P. Zehr, and K. S. Johnson 1141 (2007), Nitrogen fixation by unicellular diazotrophic cyanobacteria in the 1142 temperate oligotrophic North Pacific Ocean, *Limnol. Oceanogr.*, 52(4), 1143 1317–1327.
- Robinson, R. S., and D. M. Sigman (2008), Nitrogen isotopic evidence for 1144 a poleward decrease in surface nitrate within the ice age Antarctic, *Quat. 1145 Sci. Rev.*, 27(9–10), 1076–1090, doi:10.1016/j.quascirev.2008.02.005.
- Sañudo-Wilhelmy, S. A., A. B. Kustka, C. J. Gobler, D. A. Hutchins, 1146 M. Yang, K. Lwiza, J. Burns, D. G. Capone, J. A. Raven, and E. J. 1147 Carpenter (2001), Phosphorus limitation of nitrogen fixation by *Tricho- 1148 desmium* in the central Atlantic Ocean, *Nature*, 411, 66–69, 1149 doi:10.1038/35075041.
- Schmittner, A., A. Oschlies, H. D. Matthews, and E. G. Galbraith (2008), 1150 Future changes in climate, ocean circulation, ecosystems, and biogeo- 1151 chemical cycling simulated for a business-as-usual CO_2 emission scenar- 1152 io until year 4000 AD, *Global Biogeochem. Cycles*, 22, GB1013, 1153 doi:10.1029/2007GB002953.
- Sigman, D. M., M. A. Altabet, R. Michener, D. C. McCorkle, B. Fry, and 1154 R. M. Holmes (1997), Natural abundance-level measurement of the nitro- 1155 gen isotopic composition of oceanic nitrate: An adaptation of the ammo- 1156 nia diffusion method, *Mar. Chem.*, 57(3–4), 227–242, doi:10.1016/ 1157 S0304-4203(97)00009-1.
- Sigman, D. M., M. A. Altabet, D. C. McCorkle, R. Francois, and G. Fischer 1158 (1999), The $\delta^{15}\text{N}$ of nitrate in the Southern Ocean: Consumption of nitrate 1159 in surface waters, *Global Biogeochem. Cycles*, 13(4), 1149–1166, 1160 doi:10.1029/1999GB900038.
- Sigman, D. M., R. Robinson, A. N. Knapp, A. van Green, D. C. McCorkle, 1161 J. A. Brandes, and R. C. Thunell (2003), Distinguishing between water 1162 column and sedimentary denitrification in the Santa Barbara Basin using 1163 the stable isotopes of nitrate, *Geochem. Geophys. Geosyst.*, 4(5), 1040, 1164 doi:10.1029/2002GC000384.
- Sigman, D. M., J. Granger, P. J. DiFiore, M. F. Lehmann, R. Ho, G. Cane, 1165 and A. van Green (2005), Coupled nitrogen and oxygen isotope measure- 1166 ments of nitrate along the eastern North Pacific margin, *Global Biogeo- 1167 chem. Cycles*, 19, GB4022, doi:10.1029/2005GB002458.
- Simmons, H. L., S. R. Jayne, L. C. S. Laurent, and A. J. Weaver (2004), 1168 Tidally driven mixing in a numerical model of the ocean general circula- 1169 tion, *Ocean Modell.*, 6(3–4), 245–263, doi:10.1016/S1463-5003(03) 1170 00011-8.
- Somes, C. J. (2010), Nitrogen isotopes in a global ocean biogeochemical 1171 model: Constraints on the coupling between denitrification and nitrogen 1172 fixation, M.S. thesis, Oregon State Univ., Corvallis.
- Thamdrup, B., and T. Dalsgaard (2002), Production of N_2 through anaero- 1173 bic ammonium oxidation coupled to nitrate reduction in marine sedi- 1174 ments, *Appl. Environ. Microbiol.*, 68(3), 1312–1318, doi:10.1128/ 1175 AEM.68.3.1312-1318.2002.
- Tyrell, T. (1999), The relative influences of nitrogen and phosphorus 1176 on oceanic primary production, *Nature*, 400, 525–531, doi:10.1038/ 1177 22941.
- Voss, M., J. W. Dippner, and J. P. Montoya (2001), Nitrogen isotope pat- 1178 terns in the oxygen-deficient waters of the eastern tropical North Pacific, 1179 *Deep Sea Res., Part I*, 48(8), 1905–1921, doi:10.1016/S0967-0637(00) 1180 00110-2.
- Wada, E. (1980), Nitrogen isotope fractionation and its significance in bio- 1181 geochemical processes occurring in marine environments, in *Isotope 1182 Marine Chemistry*, edited by E. D. Goldberg et al., pp. 375–398, Uchi- 1183 da-Rokakuho, Tokyo.

- 1203 Wada, E., and A. Hattori (1978), Nitrogen isotope effects in the assimila- 1218
 1204 tion of inorganic nitrogenous compounds by marine diatoms, *Geomicro-* 1219
 1205 *biology J.*, *1*(1), 85–101, doi:10.1080/01490457809377725.
- 1206 Waser, N. A. D., P. J. Harrison, B. Nielsen, S. E. Calvert, and D. H. Turpin 1220
 1207 (1998), Nitrogen isotope fractionation during the uptake and assimilation 1221
 1208 of nitrate, nitrite, ammonium, and urea by a marine diatom, *Limnol.* 1222
 1209 *Oceanogr.*, *43*(2), 215–224, doi:10.4319/lo.1998.43.2.0215.
- 1210 Weaver, A. J., et al. (2001), The UVic Earth system climate model: Model 1223
 1211 description, climatology, and applications to past, present and future cli- 1224
 1212 mates, *Atmos. Ocean*, *39*(4), 361–428. 1225
- 1213 Wu, J., W. Sunda, E. A. Boyle, and D. M. Karl (2000), Phosphate depletion 1226
 1214 in the western North Atlantic Ocean, *Science*, *289*, 759–762, 1227
 1215 doi:10.1126/science.289.5480.759.
- 1216 Zehr, J. P., J. B. Waterbury, P. J. Turner, J. P. Montoya, E. Omoregie, G. F. 1228
 1217 Steward, A. Hansen, and D. M. Karl (2001), Unicellular cyanobacteria 1229
 fix N₂ in the subtropical North Pacific Ocean, *Nature*, *412*, 635–638, 1230
 doi:10.1038/35088063. 1231
 M. A. Altabet, School for Marine Science and Technology, University of 1232
 Massachusetts Dartmouth, North Dartmouth, MA 02747, USA.
 A. Bourbonnais and M. Eby, School of Earth and Ocean Sciences, 1222
 University of Victoria, Victoria, BC V8W 2Y2, Canada. 1223
 E. D. Galbraith, Department of Earth and Planetary Science, McGill 1224
 University, Montreal, QC H3A 2T5, Canada. 1225
 M. F. Lehmann, Institute for Environmental Geoscience, University of 1226
 Basel, CH-4003 Basel, Switzerland. 1227
 R. M. Letelier, A. C. Mix, A. Schmittner, and C. J. Somes, College of 1228
 Oceanic and Atmospheric Sciences, Oregon State University, Corvallis, 1229
 OR 97331, USA. (csomes@coas.oregonstate.edu) 1230
 J. P. Montoya, School of Biology, Georgia Institute of Technology, 1231
 Atlanta, GA 30332, USA. 1232

Article in Proof